Experimental Analysis of Low Altitude Terrain Following for Hover Capable Flight Style Autonomous Underwater Vehicles

Sophia M. Schillai
Fluid Structure Interactions Group
University of Southampton
Boldrewood Innovation Campus
Southampton, S016 7QF
sms4g13@soton.ac.uk

Stephen R. Turnock
Fluid Structure Interactions Group
University of Southampton
Boldrewood Innovation Campus
Southampton, S016 7QF
S.R.Turnock@soton.ac.uk

Eric Rogers
Electronics and Computer Science
University of Southampton
University Road,
Southampton, SO17 1BJ
etar@ecs.soton.ac.uk

Alexander B. Phillips
National Oceanography Centre
European Way,
Southampton, SO14 3ZH
abp@noc.ac.uk

Abstract

Operating an AUV in close proximity to terrain typically relies solely on the vehicle sensors for terrain detection, and challenges the manoeuvrability of energy efficient flight style autonomous underwater vehicles. This paper gives new results on altitude tracking limits of such vehicles by using the fully understood environment of a lake to perform repeated experiments while varying the altitude demand, obstacle detection, and actuator use of a hover capable flight style AUV. The results are analysed for mission success, vehicle risk, and repeatability, demonstrating the terrain following capabilities of the overactuated AUV over a range of altitude tracking strategies and how these measures better inform vehicle operators. A major conclusion is that the effects of range limits, bias, and false detections of the sensors used for altitude tracking must be fully accounted for to enable mission success. Furthermore it was found that switching between hover and flight style actuation based on speed, whilst varying the operation speed, has advantages for performance improvement over combining hover and flight style actuators at high speeds.

1 Introduction

For applications such as monitoring the adverse effects of climate change (Ling et al., 2016), managing food supply (Smale et al., 2012; Nishida et al., 2014a), or understanding the impact of mining activity at the seafloor (Nakajima et al., 2015), photographic surveys taken with AUVs can not only enhance existing approaches, or reliably perform repeat surveys (Nakajima et al., 2015; Smale et al., 2012) but also replace alternatives that are damaging to the survey area or that put human divers at risk (Smale et al., 2012).
To perform surveys at a low altitude, the AUV faces particular sensor, planning, and control challenges. Information about the terrain ahead must be obtained together with the vehicle state relative to the ter-

rain ahead. Also the correct control actions for achieving the goal altitude or avoiding an obstacle whilst maintaining a constant forwards speed must be computed and applied.

This paper explores the use of a small scale test platform for larger hover capable and flight style AUVs to perform repeated cost and time efficient studies on terrain following. It gives new results on low altitude terrain following strategies for a torpedo style hover capable AUV, operating over a range of forwards speeds and altitudes.

In the next section, background on low altitude terrain tracking is given. Then in Section 3 the information available on vehicle performance in existing photographic missions is reviewed, focusing on the Autosub6000 vehicle (McPhail et al., 2010). This is followed in Section 4 by a description of the re-implementation of the terrain detection, horizon tracking and altitude control of Autosub6000 on the hover capable Delphin2, together with the integration of the hover capability in the altitude control.

The two vehicles considered are shown in Figure 1 and are of similar hull design, but different scales, and their outlines are compared in Figure 2 (normalised by length). The experiments performed with Delphin2 to test and evaluate the altitude tracking reliability, repeatability and collision safety are described in Section 5. Section 6 gives the results of this analysis. The impact of range limitations and measurement errors of the altimeter and scanning sonar on the repeatability and collision risk are identified and the addition of thruster actuation at full speed is demonstrated to be detrimental to the vehicle controllability. To better inform vehicle operators, the relationship between collision risk, photographic mission success and vehicle endurance is explored. Based on this research, the detection of the terrain ahead is identified as the key challenge for increasing the survey speed in the current configuration of the Delphin2 AUV. Conclusions are drawn in Section 7 and possible areas for further research discussed.

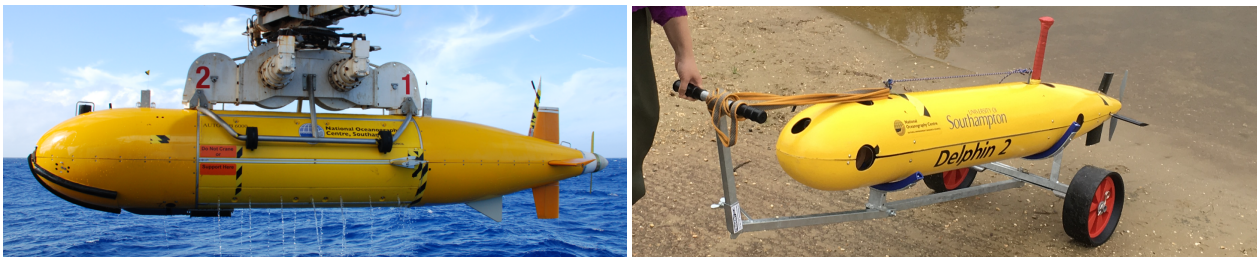

(a) (b)

Figure 1: Autosub6000 and Delphin2, the two AUVs considered in this paper.

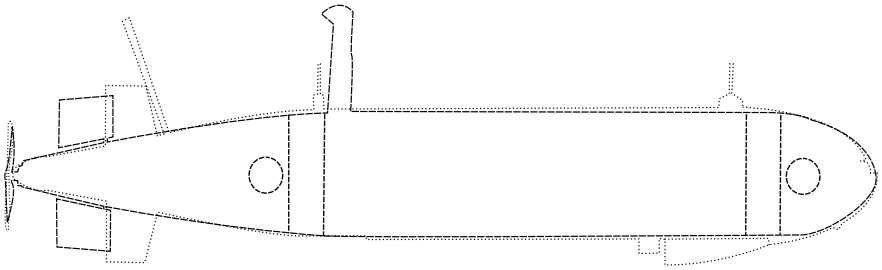

Figure 2: Side view shape comparison of the Autosub6000 (dotted lines) and Delphin2 (dashed lines) AUVs.

2 Background

Typically, AUVs performing photographic missions are optimised for either range or manoeuvrability. Long endurance flight style vehicles use sternplanes to control the vehicle heading and pitch and a main propeller at the rear to maintain forwards speed. They are optimised for range and endurance, but are limited in their capability to avoid obstacles (Houts et al., 2012; McPhail et al., 2010).

A reduction in operating speed comes at the cost of reducing the maximum achievable pitch angle and increasing the required pitch to keep a constant depth (Eng and Chitre, 2015). The more manoeuvrable hover capable AUVs are typically fitted with thrusters, providing actuation with more degrees of freedom and were used in initial proposals for AUV based photographic surveys (Haywood, 1986; Yoerger et al., 1991). Operating safely in complex terrains and with a requirement to undertake surveys of well defined areas of interest (e.g. archeological ship wreck surveys (Gracias et al., 2013; Roman and Mather, 2010)), the lower operational speeds (Smale et al., 2012; Marouchos et al., 2015; Nishida et al., 2014b; Gracias et al., 2013) combined with the power consumption of the thrusters increases the time and energy cost per covered area (Smale et al., 2012; Nishida et al., 2015). Attempting to compromise between the two options, several hover enhanced flight style vehicles have been developed, e.g. (Wynn et al., 2014; Phillips et al., 2013; Packard et al., 2010).

Low altitude AUV surveys vary widely in water depth, survey altitude, and the size of the survey area, from grids over a 25 m×25 m area at 15 m depth and less (Smale et al., 2012) to large scale grids over a 10 km×10 km area at 5000 m depth (Morris et al., 2014). Limited by the location specific light attenuation and scattering of light in water (Jaffe, 1990; Akkaynak et al., 2017), available means of lighting and required image resolution, the required survey altitude is always very low. In practice altitude demands vary between 0.4 m and 12 m (Yoerger et al., 2007; Marouchos et al., 2015; Bodenmann et al., 2013; Houts and Rock, 2015; Morris et al., 2014).

Generally, vehicle path planning is split between the vertical and horizontal planes. In the horizontal plane, the waypoints are typically evenly spaced in a grid, as required by sampling strategies or for a large area reconstruction (Smale et al., 2012; Morris et al., 2014), and although recent work investigates more complex path planning in the horizontal plane (Otsuki et al., 2016), a separation of horizontal waypoints and vertical altitude goals remains. This allows the simplification of obstacle avoidance to a two dimensional problem.

Typically, the engineering data and the photo analysis are treated independently. This produces a report if a collision occurrs and how tall a step was successfully navigated, and separately a total number of photos or a total area that was successfully mapped without investigating the detailed vehicle state for the less successful photos.

3 Existing Terrain Following Strategies

Pre-deployment planning based on existing maps can improve the altitude tracking results and vehicle safety (Houts and Rock, 2015) but its applicability is limited since for most of the ocean no high resolution maps are available (Becker et al., 2009; Harris et al., 2014). Most vehicles rely on in-situ measurements for terrain detection in the vertical plane. If the water quality allows it, camera systems can be used for obstacle detection (Marouchos et al., 2015), but sonar sensors are more widely used due to their longer range capability and lower sensitivity to water quality.

Sensor configurations include downwards altimeter only (Steenson et al., 2014), mechanical scanning sonar (McPhail et al., 2010) or multibeam sonar (Houts and Rock, 2015). The range measurement is performed in discrete time steps, so-called 'bins'. Based on the speed of sound in water, a distance can be assigned to each bin. When using a single beam or mechanical scanning sonar, the device sends a single acoustic pulse through the water. The acoustic pulse has approximately cone-shaped, with a given vertical and horizontal opening

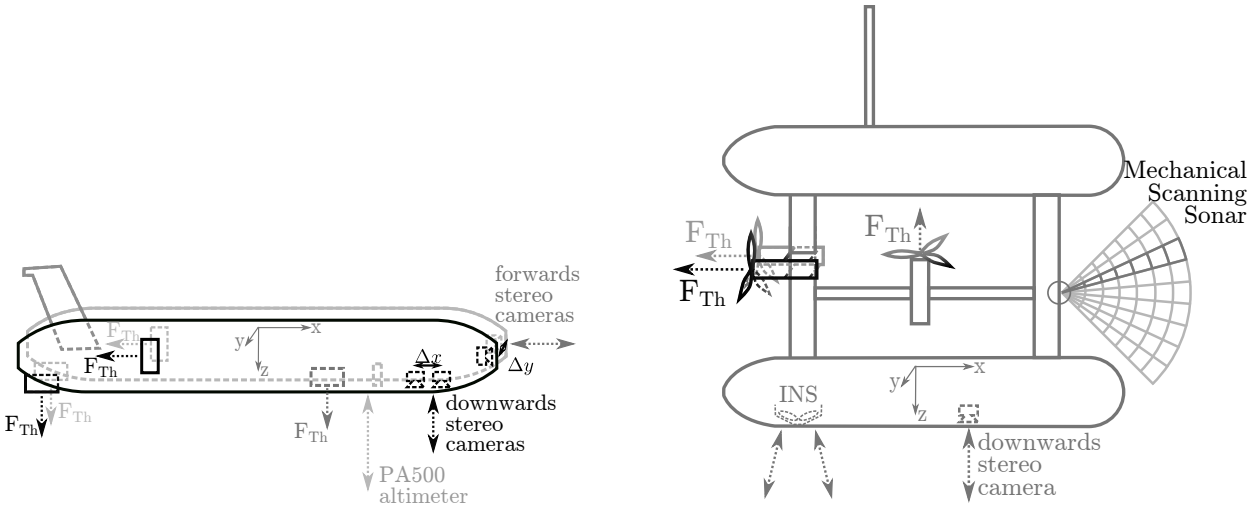

Figure 3: Side view drawings of hover-style low altitude terrain tracking AUVs. Cameras and altitude tracking sensors and actuators are indicated where known. Greyscale alludes to position in the y-direction.

angle. For the mechanical scanning sonar, the angle position of the sonar head can be configured within one plane of rotation. Detecting an obstacle on the returns of a single beam or mechanical scanning sonar involves analysing the numbers representing the return intensity in each bin to establish at which distance an obstacle is reflecting sound. Algorithms for such detection include using a fixed, constant threshold above which a return is considered an obstacle, automated threshold detection e.g. using Otsu thresholding (Chew and Chitre, 2013), or through a first-order infinite impulse response digital filter (McPhail et al., 2010). More complex analysis methods model the sound propagation within the sonar beam to calculate a probability of occupancy for a grid map (Zhou et al., 2016).

Altitude tracking capabilities are often mentioned, but detailed information on the performance is rarely available; often key information like survey speed, obstacle detection sensor details, or information on the navigated terrain are omitted. The four classes of AUV described in more detail below were selected for the detail of information available on their terrain tracking ability or the demonstration of terrain tracking below 10 m altitude in application.

The Starbug AUV and SeaBED AUV are both less than 2 m long thruster actuated AUVs. Both are constructed of two torpedo shaped hulls, but with different alignment (see Figure 3). The original Starbug Mk3 AUV was designed to investigate navigation based on optical light and further developed into the Starbug X AUV which operates in shallow, clear water. The stereo cameras used for downwards and forwards terrain detection have a detection range of 0.2 m to 1.7 m (Dunbabin et al., 2005). In addition to the stereo cameras, a Tritech PA500 sonar altimeter with a minimum altitude of 0.1 m and a resolution of 0.001 m is used for altitude measurements. The goal altitude for imaging is between 0.4 m and 0.9 m (Marouchos et al., 2015). At a survey speed 0.6 m/s, with an endurance of 10 hours it can achieve a range of approximately 22 km (Marouchos et al., 2015).

The SeaBED AUV was designed for low altitude surveys at the Woods Hole Oceanographic Institution (Singh et al., 2004b). Photographic missions with the SeaBED AUV and its derivatives Mola Mola and Sirius are well documented (Tolimieri et al., 2008; Williams et al., 2009b; Woolsey et al., 2009; Singh et al., 2004a; Bingham et al., 2010; Williams et al., 2010a; Williams et al., 2010b; Williams et al., 2009a), however technical details on the altitude tracking are not so well reported. It uses a Proportional plus Integral plus Derivative (PID) depth control for altitude tracking, combining altimeter and depth measurements to obtain a depth demand. The Sirius AUV has been enhanced with a Tritech Micron mechanical scanning sonar for forwards detection (personal communication S. Williams, June 2018). The AUVs operate at speeds between 0.3 m/s and 1 m/s, at up to 2000 m depth (Singh et al., 2004a). The surveyed terrain structures include a 75^o

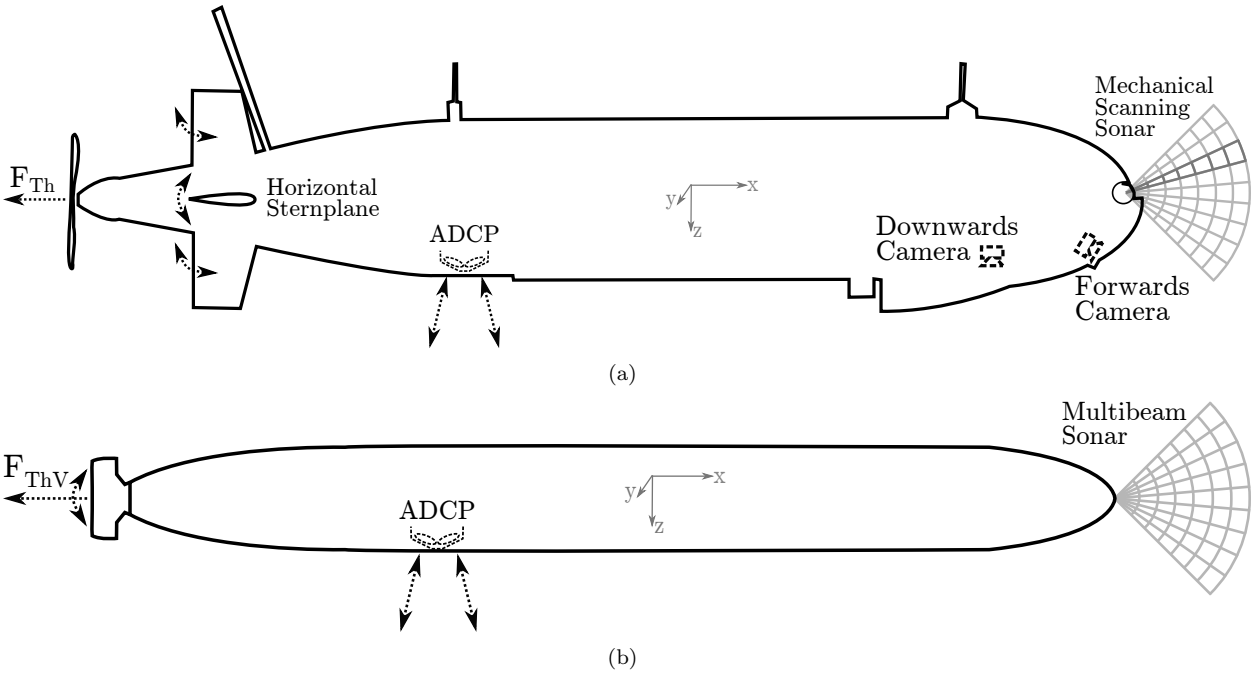

Figure 4: Side view drawings of flight style AUVs used in existing terrain following work. Cameras, altitude tracking sensors, and actuators are indicated where they could be identified from publications.

slope at 3m altitude and 0.3m/s speed, limited in speed by the required image overlap (Singh et al., 2004a). Plots of the vehicle path over terrain are included in (Singh et al., 2004a; Singh et al., 2004b), however the vertical exaggeration of the terrain makes it difficult to read details of the altitude tracking results from the plots. With the battery capacity allowing an average endurance of 8 hours, the track length achievable within one mission is between 8.6km at 0.3m/s, and 28.8km at 1.0m/s.

The Autosub6000 AUV and Dorado class AUVs are almost 6m long flight style vehicles, that are also capable of operation at low altitudes. A side view drawing comparing the vehicle outlines and key sensor positions is shown in Figure 4. The initial obstacle detection of both vehicles is based on the horizon tracking method first developed for Autosub6000, relying on a mechanical scanning sonar. Surveys using this algorithm have been performed at altitudes between 3m and 20m at a speed of 1m/s (McPhail et al., 2010; Houts et al., 2012).
The Dorado obstacle avoidance system has been extended for application in areas where maps are available beforehand. Relying on terrain relative navigation for accurate positioning, the knowledge of the area ahead is used to pre-plan trajectories at an altitude between 2m and 4m. Should unexpected obstacles be detected with the scanning sonar, the planned trajectories are overwritten by the reactive horizon tracking control (Houts et al., 2012). The work has been further improved by including uncertainty in the trajectory planning, and by upgrading the forwards detection sensor to a multibeam sonar. Existing publications report simulations based on terrain data from previous missions, obtaining an effective turning radius of 17m and a maximum pitch angle of 45^o as altitude tracking limits; (Houts and Rock, 2015) compares three avoidance planning strategies on the example of an approximately 50m high terrain step.

3.1 Autosub6000

Autosub6000 is a flight style vehicle developed and operated by the National Oceanograpy Centre Southampton (UK). The 5.5m long vehicle was developed based on the hull shape of the Autosub1 design which has been studied in detail using model experiments and simulation (Kimber and Marshfield, 1993; Phillips et al.,

2010). For better protection in case of terrain collisions, Autosub6000 was reinforced with a skid panel and fender assembly (McPhail, 2010) (see outline Figure 2). Autosub6000 has performed several large area, low altitude missions at 3 m to 10 m altitude e.g. during the Autosub6000 development cruise D343 (McPhail, 2010; McPhail et al., 2010) and the research cruise D377, studying the Porcupine Abyssal Plain (Ruhl, 2013; Morris et al., 2014). One photographic mission can be over 15 hours long and have a survey length of over 90 kilometres. Table 1 includes key vehicle and mission parameters of Autosub6000.

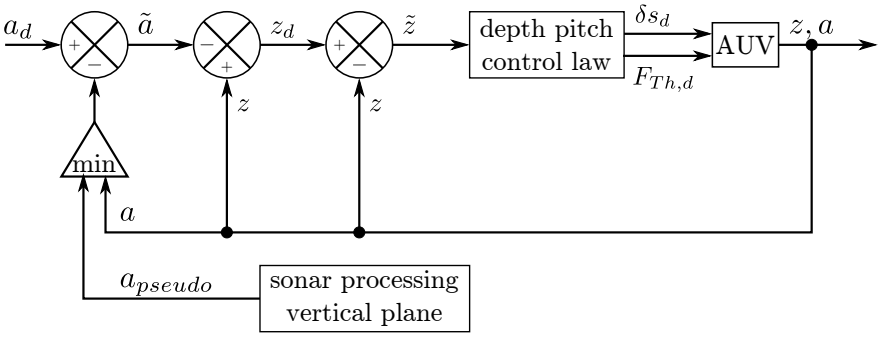

Figure 5: Conversion of the altitude demand a_d and the depth (z), altitude (a) and pseudo altitude (a_{pseudo}) sensor information for use in the existing depth control on Autosub6000 and Delphin2.

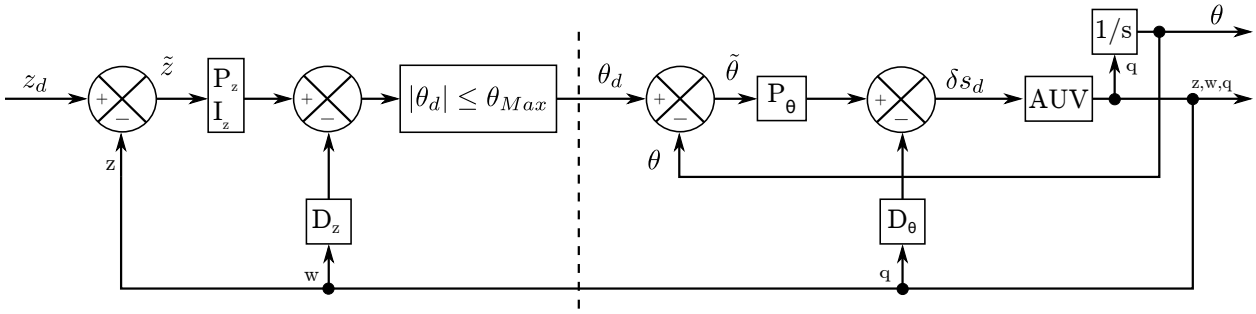

Figure 6: Cascaded depth-pitch PID control of Autosub6000, based on (McPhail and Pebody, 1998; Pebody, 2008) and code extracts.

The obstacle avoidance was added onto the existing system using a Seaking mechanical scanning sonar mounted to scan the vertical plane ahead of the vehicle. The angular position of the sonar head is adjusted after each measurement, based on whether the seafloor was successfully detected in the previous measurement, thus tracking the horizon with the scan angle. Should no terrain be detected at any of the sonar settings, the scans continue over the lower half of the available sonar angles. The terrain returns are detected with a digital impulse filter (Furlong et al., 2009), due to the non-ideal shape of the sonar beam a filter for returns from sidelobes was added. From that highest angle at which the seabed is still detected, an auxiliary parameter, called the "pseudo altitude" a_{pseudo} is calculated (similar to the illustration in Fig. 8 (a)). The pseudo altitude a_{pseudo} is then compared to the current altitude a of the vehicle. The smaller value of the two is used to calculate the altitude error $\tilde{a}$ to the altitude demand a_d. This altitude error combined with the current depth z is used to calculate a depth demand z_d (see Figures 5, 6), which is then used in the existing depth control loop, a cascaded PID control that is shown in 5. In addition to this general system, on Autosub6000 further steps are implemented to filter the sonar returns for misleading returns from sidelobes of the sonar beam, and to trigger an avoidance manoeuvre in the horizontal plane by raising a 'collision immanent' flag (McPhail et al., 2010).

Despite the obstacle avoidance system, a small number of collisions occurred when tracking the seabed with Autosub6000 and during several missions the achieved altitude was several metres above the goal altitude. However, trying to improve the system on Autosub6000 requires understanding a complex system, whilst limited in the tests that can be performed. Due to the size of Autosub6000 tests can only be performed at sea, operating from a ship, which is associated with large costs and a high risk to the AUV. Recorded mission

data exists, but simulation tests can only use the collected in-situ data and the engineering details that were recorded at the time. An accurate simulation for altitudes below 10m is difficult to achieve since due to the focus on the photographic data often engineering parameters were not recorded in sufficient detail, the actual terrain structure is only known as far as it can be re-constructed from the on-board sensor data, and suggested sensor and actuator changes can not be validated without costly and time consuming changes to the vehicle.
This paper demonstrates the use of Delphin2, a small scale model of Autosub6000, as a cost efficient and easy to deploy test platform to better understand the challenges of low altitude terrain following with flight style AUVs. It evaluates concepts for improving vehicle safety and photographic mission success and investigates how the gained understanding can be applied back to larger style flight style AUVs.

4 Terrain following with Delphin2

Delphin2 is a 3:1 scaled model of Autosub6000 developed at the University of Southampton (Phillips et al., 2013). Figure 2 illustrates the similarity of the two hull shapes. For increased manoeuvrability, Delphin2 is additionally equipped with four through-body thrusters which allows hovering and operation at slower speeds. It has been used for altitude tracking, in Lower Lough Erne, Ireland, (Steenson et al., 2014) using a downwards facing echo sounder (altimeter) mounted in the front section of the vehicle. Delphin2 was flown at an altitude of 0.75m with a surge velocity of $0.5\,\mathrm{m\,s^{-1}}$. As a result of the lack of forwards looking situational awareness, one crash with the lakefloor occurred during those trials (Steenson et al., 2014).

To further understand the horizon tracking challenges, terrain following was added to the existing AUV control system on Delphin2 using a similar structure as developed for Autosub6000. The added system consists of three components already existing on Autosub6000: Terrain detection with the mechanical scanning sonar, horizon tracking based on the terrain detection data, and use of this data for altitude control. The choice of actuation method available on Delphin2 adds an additional component of the altitude tracking which allows comparing hover- to flight style actuation as well as evaluating if thrusters at higher speeds, albeit less efficient, can improve the survey success. The actuation force allocation is based on the surge velocity estimate. The surge dependent weight function for the actuators (further described in Section 4.4) is then applied to the actuator demands of the controller (Section 4.3). An overview of the system components is shown in Figure 7. This section describes the implementation on Delphin2, detailing the changes made relative to the Autosub6000 system due to sensor and actuation differences between the two vehicles, as well as variations in the experiment conditions.

As for Autosub6000, the vertical plane is assumed to be independent of the horizontal plane, and only vertical plane actuation and control are considered. Figure 8(b) shows the nomenclature of the vertical plane actuation and reference frame. Assuming positive surge velocity, a positive pitch angle leads to the AUV's surfacing. Moments that contribute to a positive pitch angle can be obtained by setting a positive sternplane angle or by configuring the thruster forces so the difference between the aft and front thruster, and thus the sum of their moments, is larger than zero ($0 \leq M_{aft} + M_{front} = F_{aft} \cdot l_{aft} - F_{front} \cdot l_{front}$).

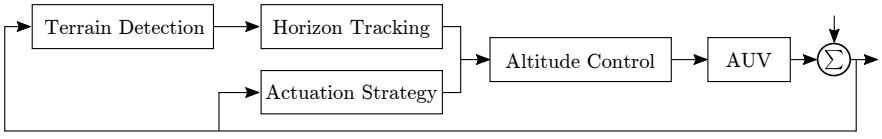

Figure 7: Block diagram illustrating the components of terrain following on Delphin2.

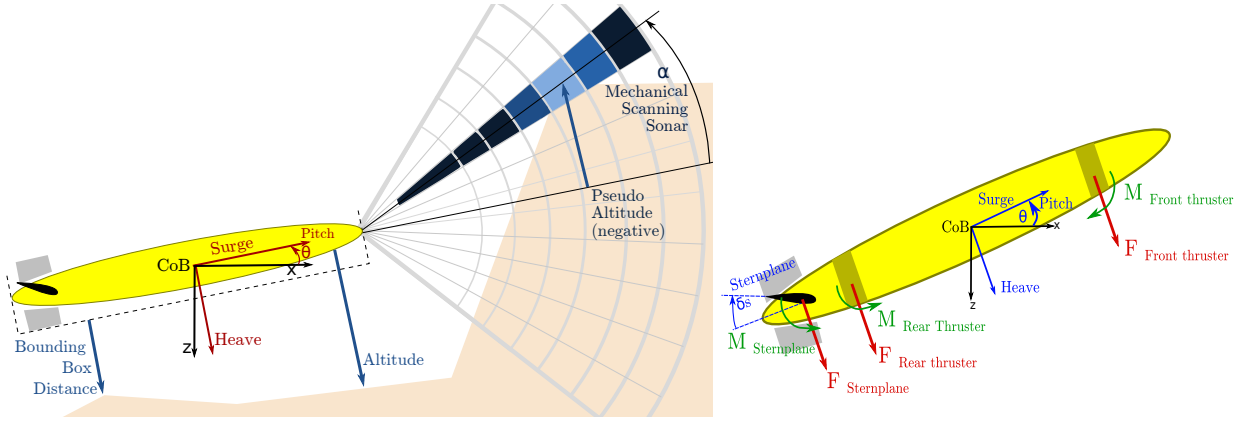

(a) (b)

Figure 8: Vertical plane navigation and obstacle avoidance of the hover capable, flight style Delphin2 AUV.

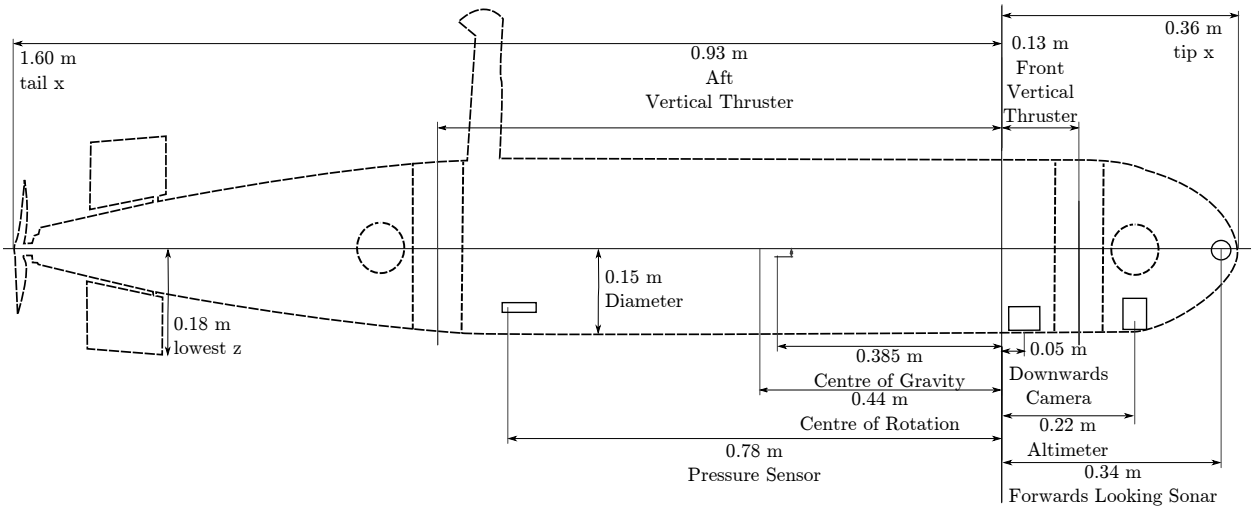

Figure 9: Sensor and actuator positions on the Delphin2 AUV.

4.1 Terrain detection

Sensors for terrain detection on Delphin2 are an altimeter, mounted downwards facing in the front section of the vehicle, and the mechanical scanning sonar, orientated to scan the vertical plane ahead. The sensors and their measuring principle are illustrated in Figure 8(a). The altimeter is a Tritech Micron Echosounder; the sonar frequency is 500 kHz, the beam shape is a 6^o conical beam. The altimeter has a minimum range of 0.5 m and a digital resolution of 1 mm (Tritech International Ltd,). The update frequency achieved with the software framework on Delphin2 is 2.5 Hz. If the altitude is less than the minimum sensor range, the altimeter returns larger readings, resulting in a terrain estimate below the actual terrain. When using only the altimeter, this increases the vehicle risk significantly, in the worst case the vehicle will try to reduce its altitude further, based on the high altimeter readings.

The mechanical scanning sonar is a Tritech Micron scanning sonar. Unlike on Autosub6000 it is operated in a continuous sector scan; further details on determining the scan pattern are given in the horizon tracking section. After choosing the sonar scanning pattern, terrain detection methods similar to those on Autosub6000 were tested on sonar data collected at Testwood lake. In the collected data no sidelobe returns as on Autosub6000 were observed. With the overall low reflectivity of the lakebed at Testwood, however,

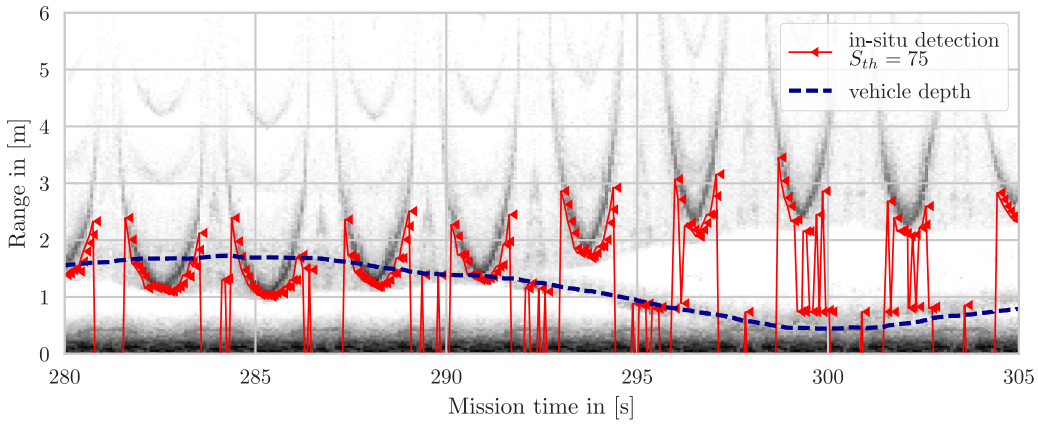

(a)

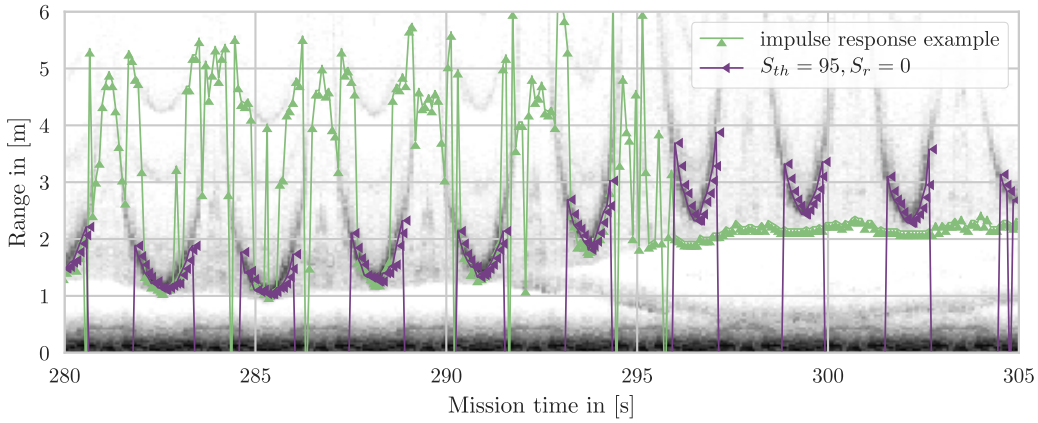

(b)

Figure 10: Terrain detection example: The sonar is continuously scanning the angle sector over time, as the vehicle moves forwards over the terrain. Each individual vertical line represents return intensities at a different scan angle. During the mission, a constant threshold of 75 was used, and returns from the water surface were mis-detected as an obstacle, resulting in the vehicle surfacing. Detection results using a higher threshold and an impulse response filter over the same sonar returns are shown in (b).

problems with water surface reflections emerged. In addition to the detection of water surface reflections when pointing the sonar beam towards the surface, a second type of water surface reflections was found to cause problems. Due to reflections within the vehicle, a portion of each sonar measurement takes a path to the water surface, causing false detection at a range roughly corresponding to the vehicle depth (see Figure 10). Combined with low reflectivity of the lakebed, the two are barely distinguishable in the returns of one measurement. Since in the experiment set-up the typical detection range for the terrain and the required vehicle depth are very similar, the option of filtering a band around the current depth was dismissed.
Several detection methods for single-beam based detections were compared to establish the most suitable method: Otsu thresholding, both with and without a reduced window size, was challenging to tune to detect a majority of correct returns, so it was omitted. A variable threshold based on an impulse response filter as on Autosub6000 could be tuned to detect terrain correctly, but the tuning was very sensitive and small changes led to missing the main return, or detection of increased noise levels. Figure 10 illustrates too long detection ranges, where the main terrain is missed, and too short detection before the main lakebed return with a parameter tuning example where both cases occur. Finally a manually selected constant sonar threshold S_{th} was tested, and found to be more reliable in detection, albeit with a detection range of only 2 m

to 4m. To increase the range further, the threshold was reduced with increasing distance to the transducer, with a total reduction of S_r per metre. Figure 10(a) shows an example from an experiment using a too low, constant threshold (case 10), resulting in the vehicle surfacing due to detecting the surface reflections as an obstacle. The same data is used for giving examples of other thresholding methods in Figure 10. For evaluation in experiments, several fixed and range dependant thresholds were chosen, with most experiments performed with a threshold of $S_{th} = 95$, resulting in low range but reliable detection.

4.2 Horizon tracking

With the detection range limits in the test environment, the scan speed becomes a more significant factor in the obstacle detection. Figures 11 and 12 illustrate the impact of scanning speed, vehicle speed, sonar range, vehicle altitude and step height when using a fixed sonar beam or a continuous sector scan. A step of given height is positioned at $x = 2$m, and the plots show the AUV's horizon estimate at each position.
It was found that the time taken to update the scan angle for individual measurements was too long, so instead a fixed scan sector was used. In addition to increasing scan speed and avoiding detections of the water surface, the regular scanning pattern has the advantages that it is easier to visually inspect after the experiment, all measurements are updated regulary, and false detections cannot influence the scanning angle, however the scan sector limits need re-consideration for different missions. The algorithm for detecting the horizon remains similar to Autosub6000. For each angle position of the scanning sonar, two values are stored: the detection range when the angle was last visited (-1 for no detection) and the pitch angle of the vehicle at the point of detection. For every new measurement, the highest angle with a valid detection in this table is used for estimating the height of the horizon ahead.

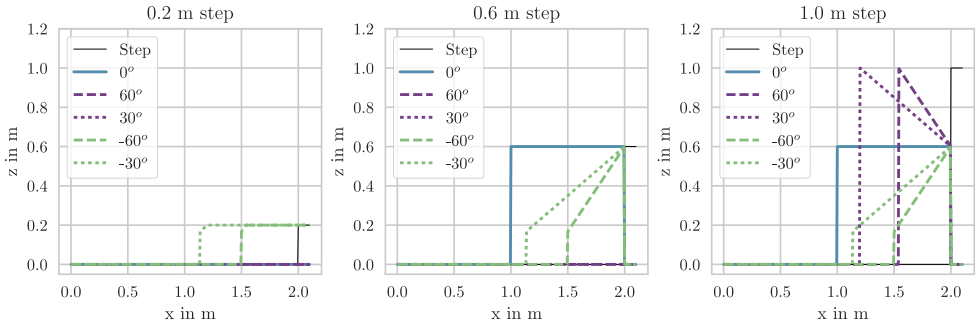

Figure 11: Detection height and range of a terrain step using constant sonar angle, altitude (0.6m), and detection range (1m) as well as zero pitch.

Figure 11 illustrates that the scanning angle limits determine how well the size of an obstacle can be determined, and how especially obstacles higher than the vehicle altitude tend to be underestimated. Expressing the obstacle height h as a pseudo altitude $a_{pseudo} = a - h$, the range Δx at which an obstacle can first be detected by a scanning sonar with range r is $\Delta x = \sqrt{r^2 - (a-h)^2}$. This assumes that the full height can actually be detected by the lowest (for small obstacles) or highest (for high obstacles) beam angle α. The detection limits for obstacle heights are $h_{min} = r \cdot \sin(\alpha_{min}) + a$ and $h_{max} = r \cdot \sin(\alpha_{max}) + a$. As the vehicle approaches, all obstacles that are not exactly the same height as the vehicle will not be detectable at full height any more. The range at which obstacles with $a - h > 0$ will be overlooked, and obstacles with $a - h < 0$ will be underestimated, is $\frac{|a-h|}{\sin(\alpha_{min/max})}$.
Transitioning from a fixed sonar to a slow scanning sonar, Figure 12 illustrates that it is detrimental for the obstacle detection that the scan period is shorter than the obstacle detection range. With a shorter scan period (increased speed of a complete sector scan, or reduced vehicle speed), the offset in terrain detection moves closer together.
A scanning sector of -60^o to 0^o and 3.6^o angle step size were chosen for the experiments to reduce the risk of falsely detecting the water surface as terrain, whilst still detecting all steps of a similar hight to the

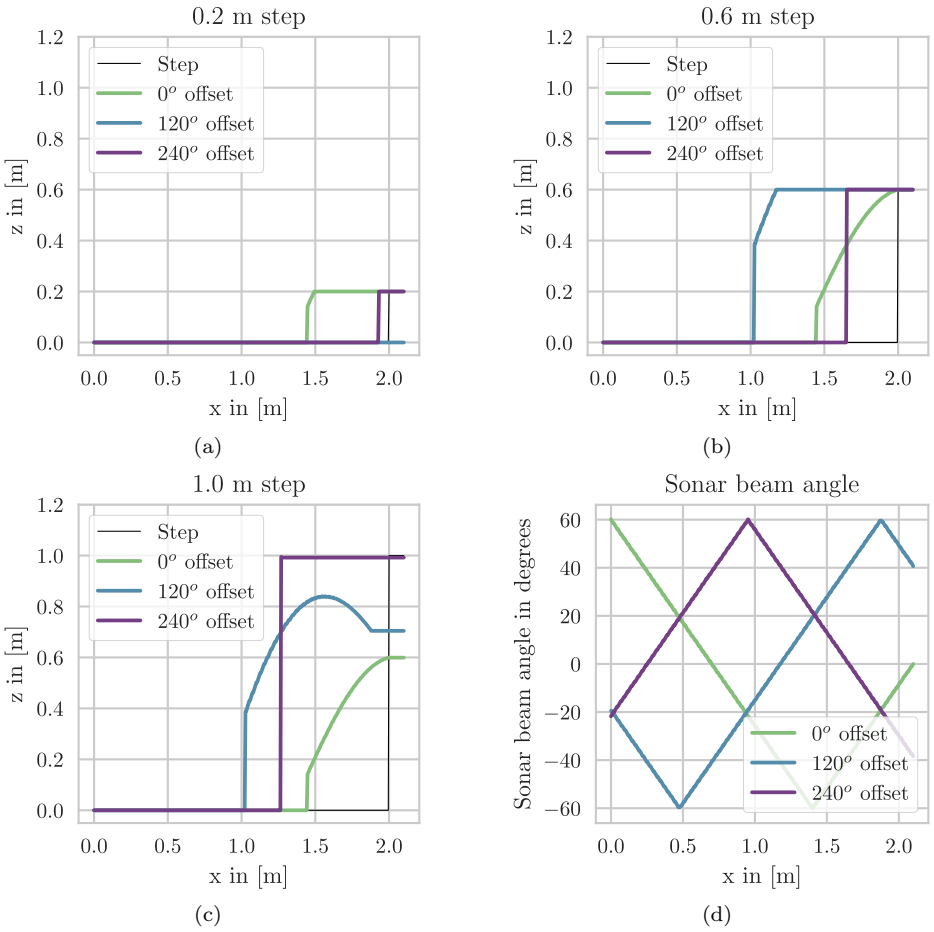

Figure 12: Detection height and range of a terrain step using a scanning sonar, scanning a sector between -60^o and 60^o, with a scan period of 2.8s at 1m/s surge speed, zero pitch angle, and varied offsets of the initial scan angle. AUV altitude 0.6m, detection range 1m.

goal altitude. To maximise the speed of one full sector scan, a step angle of 3.6^o was chosen (above the recommended maximum step size of 1.8^o). At this step size, the speed per degree is $0.023\frac{\text{s}}{1^o}$ (4.1s for a 90^o sector scan period). The resulting time for a full scan with 3.6^o steps is 2.8s. In the same time, a horizon scanning beam pattern would complete 3.5 measurements, covering a maximum section of 12^o.

4.3 Altitude controller

Previous studies into the depth tracking performance of Delphin2 have utilised model predictive control (Steenson et al., 2014) and a cascaded PID controller (Tanakitkorn et al., 2016). For this study the cascaded PID depth controller was utilised due to its similarities to the control on Autosub6000. Unlike on Autosub6000, the existing PID control scheme on Delphin2 is a combination of hover capable and flight style control, unified to work over a range of operation speeds. The contribution of the thrusters and horizontal sternplanes is allocated by applying a weighting function based on the forwards speed. The full control design is shown in Figure 13, with the split of flight style control (top) and hover capable control marked.

For the altitude tracking experiments, the altimeter was used as the only input of the depth controller. The depth demand was calculated from the current depth, the current pitch, the current altitude and the altitude demand. During the horizon tracking experiments, the altitude from the altimeter was compared

to the pseudo altitude calculated from the forwards looking sonar, and the lowest of the two values was used to calculate the depth demand.

4.4 Actuation strategy

The weight functions w_{th} for the thrusters and w_{sp} for the horizontal sternplanes are given in (1) and (2) below. During the experiments described in this paper, the weight function for the thrusters was modified for the fastest speed, to test if the altitude tracking performance could be improved by using thrusters outside their optimal speed. The used parameters for the mid-transition speeds u^*_{th} and u^*_{sp}, and the width of the transition zone are given in Figure 14, which also shows the resulting weight functions.

$$w_{th} = 1 - \frac{1}{2}\left(tanh\left(\frac{u - u^*_{th}}{\sigma^*_{th}}\right) + 1\right) \tag{1}$$

$$w_{sp} = \frac{1}{2}\left(tanh\left(\frac{u - u^*_{sp}}{\sigma^*_{sp}}\right) + 1\right) \tag{2}$$

5 Testwood Lake Experiment Setup

To test terrain following with flight style AUVs, a body of water that allows a long enough path for the vehicle to reach a steady state is required. Testwood lake, a 4 m deep reservoir north-west of Southampton, with an area of approximately 200 m by 500 m was chosen. It has a suitable very even, 300 m wide 0.6 m high step feature (see Figure 15). Further advantages of the lake environment over considered towing tanks are the lack of sonar reflections from side walls and the low magnetic disturbance to the compass.
Before tests began, a depth map of the entire lake and a detailed map of the area of interest was acquired from the water surface using GPS positioning and altimeter readings. A transect for crossing the step feature at a 90 degree angle was chosen, and a distance of 25 metres was added before and after the step to ensure the vehicle operated in a steady state when reaching the step (see Fig. 15). During the Testwood Lake experiments, the vehicle crossed the 0.7 m high that was identified in the lake, performing altitude tracking from point A to point B ($A \triangleright B$) and in the reverse direction ($B \triangleright A$). All experiments were then executed by reaching the start position at the surface with GPS fix, diving to the goal altitude with the thrusters, and then moving forwards whilst maintaining a constant heading and the chosen altitude tracking method for the selected case.

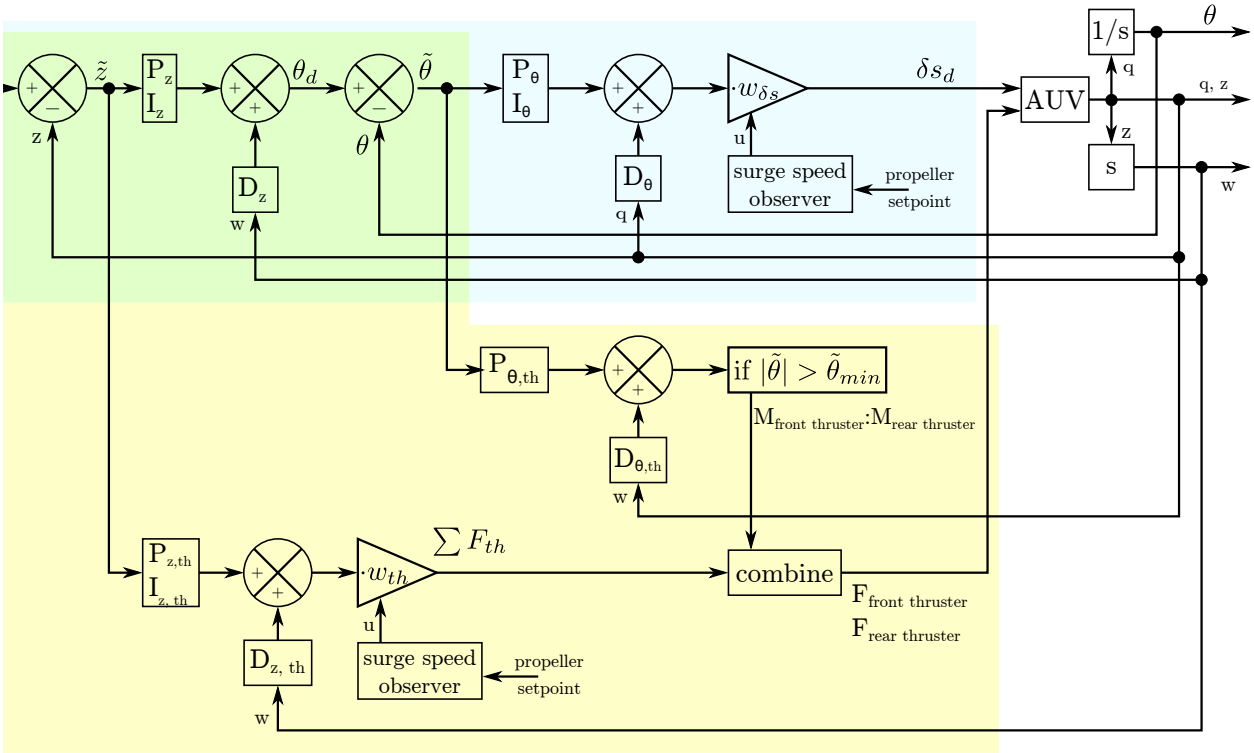

Figure 13: PID control scheme unifying flight style and hover capable actuation of Delphin2. The flight style (top) and hover style (top left, bottom) components are indicated.

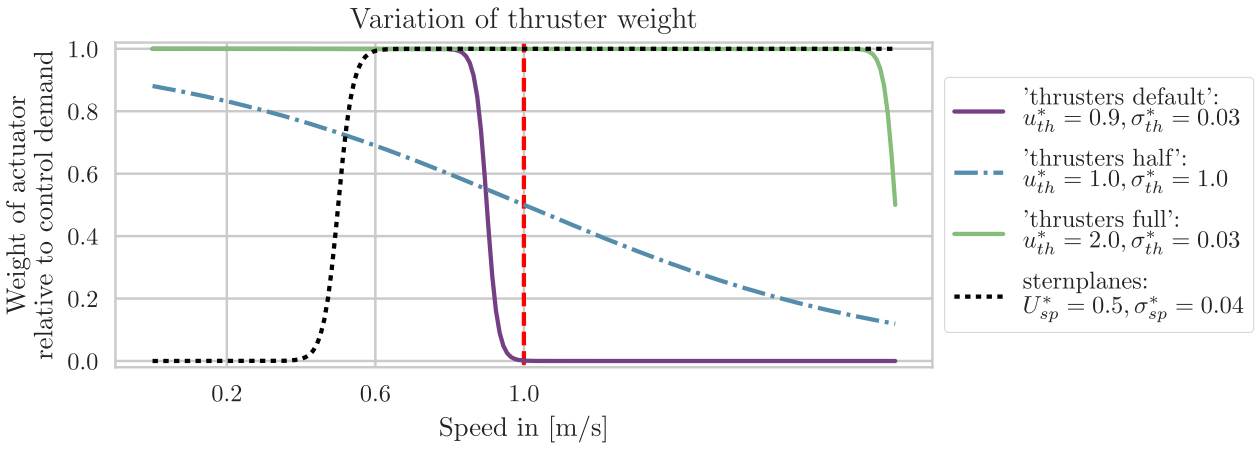

Figure 14: Thruster and sternplane weight functions: The sternplane weight function remains unchanged, the default thruster weight function is used for all three surge speeds, and the 'thrusters half' and 'thrusters full' variation is tested in cases (4) and (5), at 1 m/s surge speed.

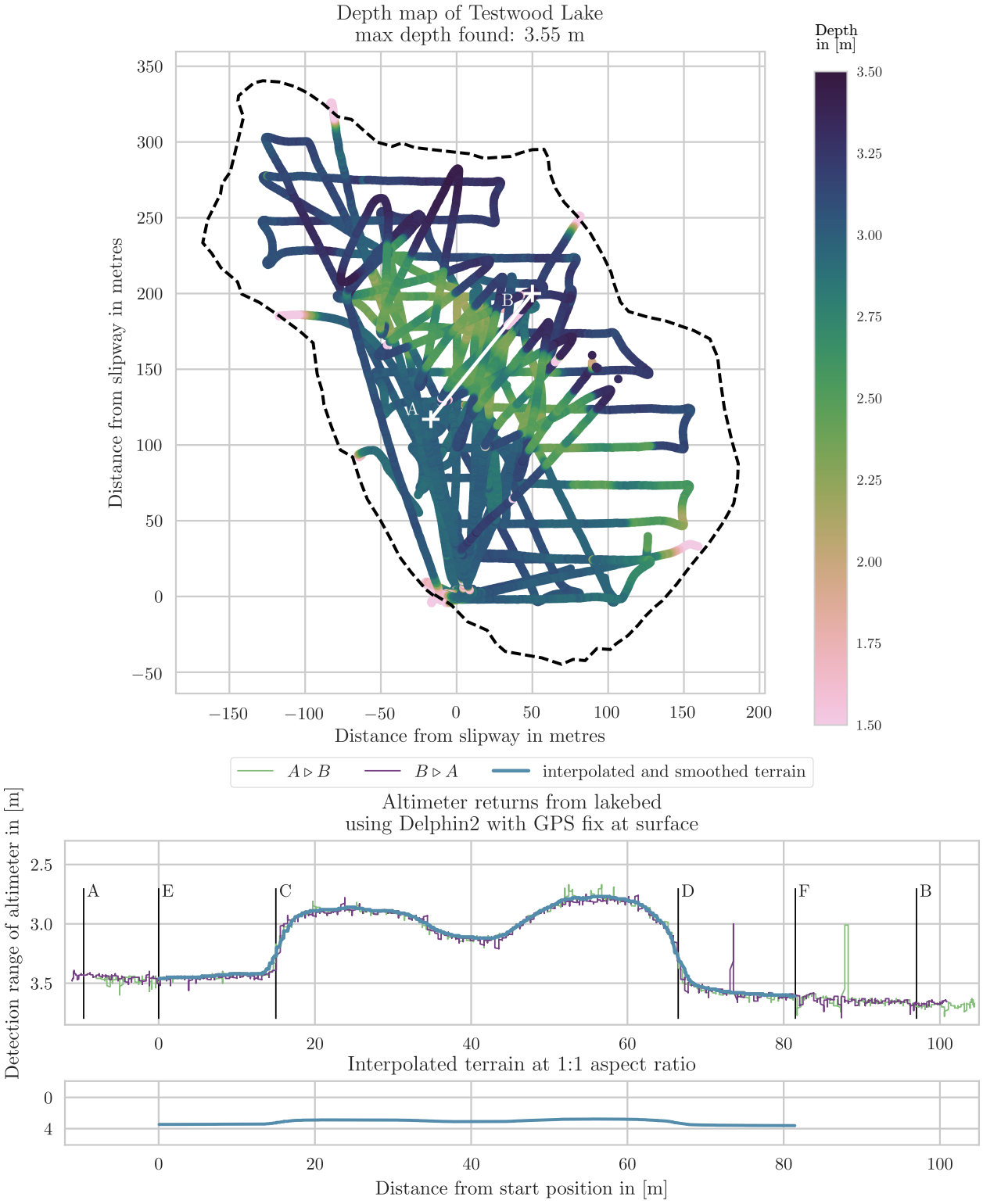

Figure 15: Testwood lake depth map and profile of the experiment path, obtained from altimeter measurements made with GPS fix at the water surface. The end points of the experiment path are A and B. The experiment path is structured with further points for analysis purposes.

5.1 Experiment parameter variation

When trying to get within an altitude region close to terrain, the vehicle operator can influence the quality of the results by modifying the goal altitude and the vehicle speed. Diving deeper into the vehicle configuration, the thruster weight and the terrain detection threshold can be used to modify the altitude tracking behaviour as well. The parameter variations were chosen to investigate the impact of those choices. 1.0 m and 0.6 m were chosen as goal altitudes for the experiments. The 1.0 m altitude is of a similar geometric scale to those used by Autosub6000 (see 1), whilst keeping the vehicle submerged throughout the path.

The lower altitude of 0.6 m was chosen to make the step a real obstacle in the path, that required avoidance. The experiment paths were crossed at 0.3 m/s, 0.6 m/s, and 1.0 m/s surge velocity. They represent low, medium, and high speeds for Delphin2 and are well understood from previous experiments on diving control (Tanakitkorn et al., 2016) and heading control at the surface (Tanakitkorn et al., 2017). During the horizon tracking experiments, the control allocation at 1 m/s speed was varied, to increase the use of thrusters from the default thruster weight of 0 to a factor of 0.5 ("half") and 1.0 ("full") (see Figure 14). All combinations of actuator settings, goal altitude, and obstacle detection settings are given in the experiment matrix (Table 2).
Two cases were identified as reference cases. To ensure repeatability, they were repeated several times, on separate days. All other experiments were only repeated twice, though sometimes these numbers vary since missions with indications of a sensor failure or an early mission abort at the lakeside were repeated as a precaution.

5.2 Performance analysis

To ensure comparability of the collected data, several steps of post processing were applied to account for changes of the water level between experiment days and restrict all data to a well defined experiment area. An estimate of the terrain shape was obtained by crossing the area of interest at the surface, using GPS for more accurate positioning. The area of interest was crossed twice, once from each direction. Based on the GPS position the distance to the start point A was calculated. Both depth maps show spikes which stem from altimeter noise. A running average was used to combine the two terrains into an estimate of the real terrain. Figure 15 shows the depth measurement from the two crossings, and the interpolated terrain estimate. To be able to compare the experiments in both directions, symmetry was achieved by including a fixed length of 15 m before and after the step, resulting in a 81.5 m long path (A to E in Figure 15). The distance between the start positions (A, B) and the considered experiment path (E, F) allows for the vehicle to reach a steady state. The recorded data was restricted to the area between the points E and F by matching the terrain estimate, obtained from the depth, pitch, and altitude during the mission, to the terrain profile obtained from the surface. This method was chosen since it was more reliable compared to acceleration based positioning. The x-position gives the distance from the start point, along the goal heading (see Figure 15).
The various sensors on Delphin2 record data asynchronously at rates between 5 Hz and 20 Hz. To combine data for calculating values derived from the sensor data, the recorded measurements were first interpolated based on the time between subsequent measurements. The terrain as seen during a mission is combined from the depth of the vehicle, the altitude, compensating the altitude based on the vehicle pitch angle. To better align the missions, the time of crossing the upwards and downwards step were read manually from a plot of the terrain as seen during the mission, over time. The error of this reading is estimated at $\pm$ 0.5 s. With a constant propeller setting and the maximum pitch angle at -20^o, the speed along the experiment path x-axis is assumed constant. With the step length read as 51.5 m, and the time between crossing the beginning and end of the step, the speed of Delphin2 along the global x-direction was estimated, cross referenced with existing speeds estimates for Delphin2 and used to estimate the x-position along the experiment path, so experiments at different speeds could be compared based on the x-position. It was found that despite attempts of normalising the depth sensor at the water surface, it had a constant error that varied by several centimetres on the same day. To compensate this offset, the mean water depth of the first section of each experiment was calculated and compared to that of the re-constructed terrain. For comparison between

different experiments, all datasets were finally interpolated and re-sampled at a resolution of 1 cm, starting at x-position $x = 0\,\text{m}$. All data post-processing relies on the python pandas library (McKinney, 2010), specifically for interpolation, re-sampling, combination and plotting of data.

Since the altimeter minimum range can cause an over-estimate of the altitude, a second altitude estimate was calculated by subtracting the depth measurement from the water depth at the estimated position. Unlike the altitude measurement from the altimeter, which is parallel to the vehicle-fixed z-axis, this altitude measurement is parallel to the global z-axis. The measurement zero is also at the bottom of the hull, and its x-position is that of the Centre of Buoyancy. Finally, a third measure for the terrain distance, first introduced in (Schillai et al., 2016) was implemented by fitting a bounding box around the Delphin2 vehicle (see Figure 8(a) for illustration and Figure 9 for the length and lowest z-coordinate of Delphin2). Using the estimate of the x-position and the terrain estimate, and considering the current pitch angle, the shortest distance of the bounding box to the terrain was used to better describe the collision risk of the entire vehicle rather than that of just a selected point. Whilst the control goal may be a constant altitude, when performing altitude tracking surveys in complex terrain, the real goal is usually to keep the survey vehicle within a suitable range of the terrain rather than at a fixed altitude. To account for this, the analysis method of risk and success zones introduced in (Schillai et al., 2016) is applied to the experiments at Testwood lake. Rather than just analysing the capability of keeping a specific altitude, a set of altitude limits, the *success zone*, is defined, within which the photographic results are deemed acceptable. For a given experiment path, the mean and standard deviation of the altitude can now be considered within those zones. The *mission success* is a direct measure what percentage/length of the path has successfully been covered by the photographic survey. In a similar manner the *risk zone* is the area within which a collision of the vehicle with the terrain is deemed likely, limited by a minimum altitude. The *mission risk* gives a direct measure of the distance spent at an altitude deemed too close to the terrain. With the altimeter failing to detect correct values below 0.4 m altitude, the risk zone was set at this altitude. Attempts were made at taking actual photos, but the algae growth in the lake was too bad to take photos of anything but shades of green, so instead the success zone was chosen to contain the space between both goal altitudes plus 0.1 m around the altitudes, resulting in a mission success zone from 0.5 m to 1.1 m. This is to compare two strategies: using a low value within the limit, or keeping the vehicle safe, but at the upper limit of the goal altitude. The goal altitudes and zone limits used for measuring the altitude tracking performance are indicated in Figure 20.

6 Results

The breadth of experiments overall was found as expected, with almost perfect altitude tracking for a hover capable, and less accurate results when pushing to higher speeds in flight style control. For all cases, the return to the goal altitude after the downwards step takes between 1.5 to 2 times longer than when navigating the step in the reverse direction. This is due to the positive buoyancy of Delphin2, and when using the forwards looking avoidance the effect is further increased due to overestimating the horizon ahead.

When taking a closer look at the sensor measurements, it can be seen how the terrain step and false detections propagate through the measured values as the AUV passes over terrain. Whilst the vehicle path looks smooth for all cases, and the altitude line only shows sensor noise of the altimeter, the impacts of sensor noise, false detections, and controller oscillation can be recognised in the altitude results after a closer look at the terrain detection sensors, the pitch angle, and the sternplane setpoints. Figure 16 is annotated to highlight this for the slowest case with hover actuation at 0.3 m/s, using the forwards looking obstacle avoidance (case 6), as well as the fastest 1.0 m/s case with flight style actuation both using the altimeter only (case 3) and using altimeter as well as forwards looking obstacle avoidance (case 8).

The next sections present a discussion of altitude tracking quality, repeatability, obstacle detection range and reliability, and impact of the actuation method. Selected cases give a more detailed insight in the factors for successful altitude tracking. Finally implications for mission planning are analysed.

6.1 Repeatability and obstacle detection

Globally, the results of the experiments are very similar within repeats of one case, whilst showing distinction between the different test cases, indicating a good repeatability and clear separation between different configurations. To further test for the repeatability of the results, the cases 8 and 14 were selected as reference cases. For each reference case, all repeats of one heading ($A \triangleright B$ or $B \triangleright A$) of that case were combined in a median line. To determine a median line for a measurement, the median of the value from each individual repeat was calculated for each point along the x-direction. The median lines are used as a reference when comparing experiments of the same case, or to compare the reference cases amongst themselves.
The mean difference of the reference cases to their own altitude median line is less than 0.1 m, with the exception of one experiment for case 8, $B \triangleright A$. This reference case is shown in Figure 17 with the special case highlighted. Whilst most of the altitude measurements only have brief individual false measurements, this case has a significant number of repeated false measurements, which lead to the vehicle increasing its altitude significantly and thus differing greatly from the other vehicle paths.

The impact of the obstacle detection parameters on the repeatability can be seen in the altitude, photographic success and risk analysis of cases 10, 11, 15, and 16, which all only differ from one of the reference cases in their sonar setting, but have a greater variation in altitude, mission success, and vehicle risk. Other experiment cases vary in their difference to the median line of the reference cases, however for most cases the repeat of the same case leads to similar results. This supports the assumption that as long as the terrain detections are correct, the experiments are very repeatable, and that a single experiment is representative of the expected performance, despite timing variation in terrain detection and unsteady control.
Extrapolating the altitude tracking results for a full battery charge and estimating the total path length that was successfully photographed, it becomes clear how much the false terrain detection can impact the photographic success, reducing the expected photographed area even below that of hover capable operation at 0.3 m/s speed for the obstacle configurations of the cases 10 and 11, rather than doubling the covered length in the case of correct detection at 1 m/s, case 8.

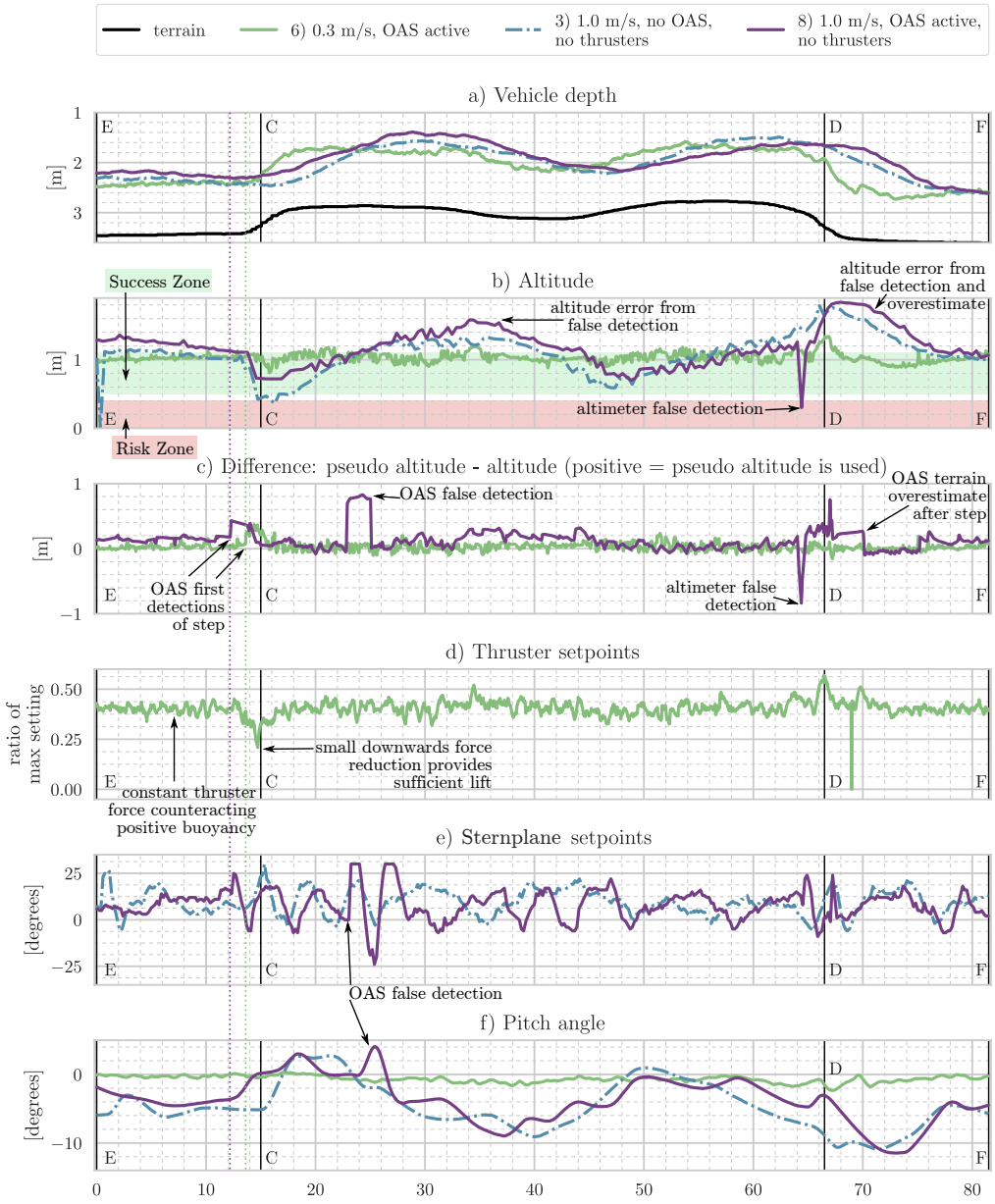

Figure 16: Comparison of terrain following performance over full terrain section for key cases, in the direction $A \triangleright B$: At slowest speed (0.3 m/s) with forwards looking obstacle avoidance (case 6), and at highest speed (1.0 m/s) with- and without forwards looking obstacle avoidance (cases 8 and 3).

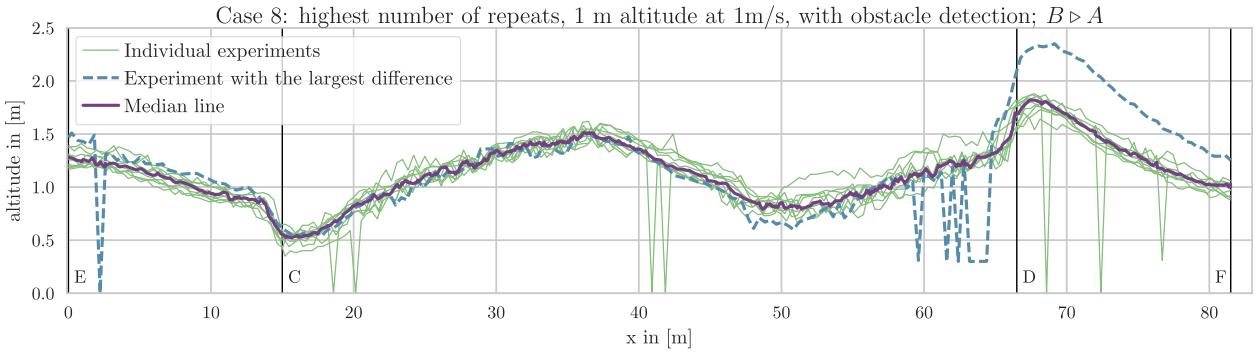

Figure 17: Comparison of the altitude median line calculated over all experiments of reference case 8, to the individual altitude recordings of case 8.

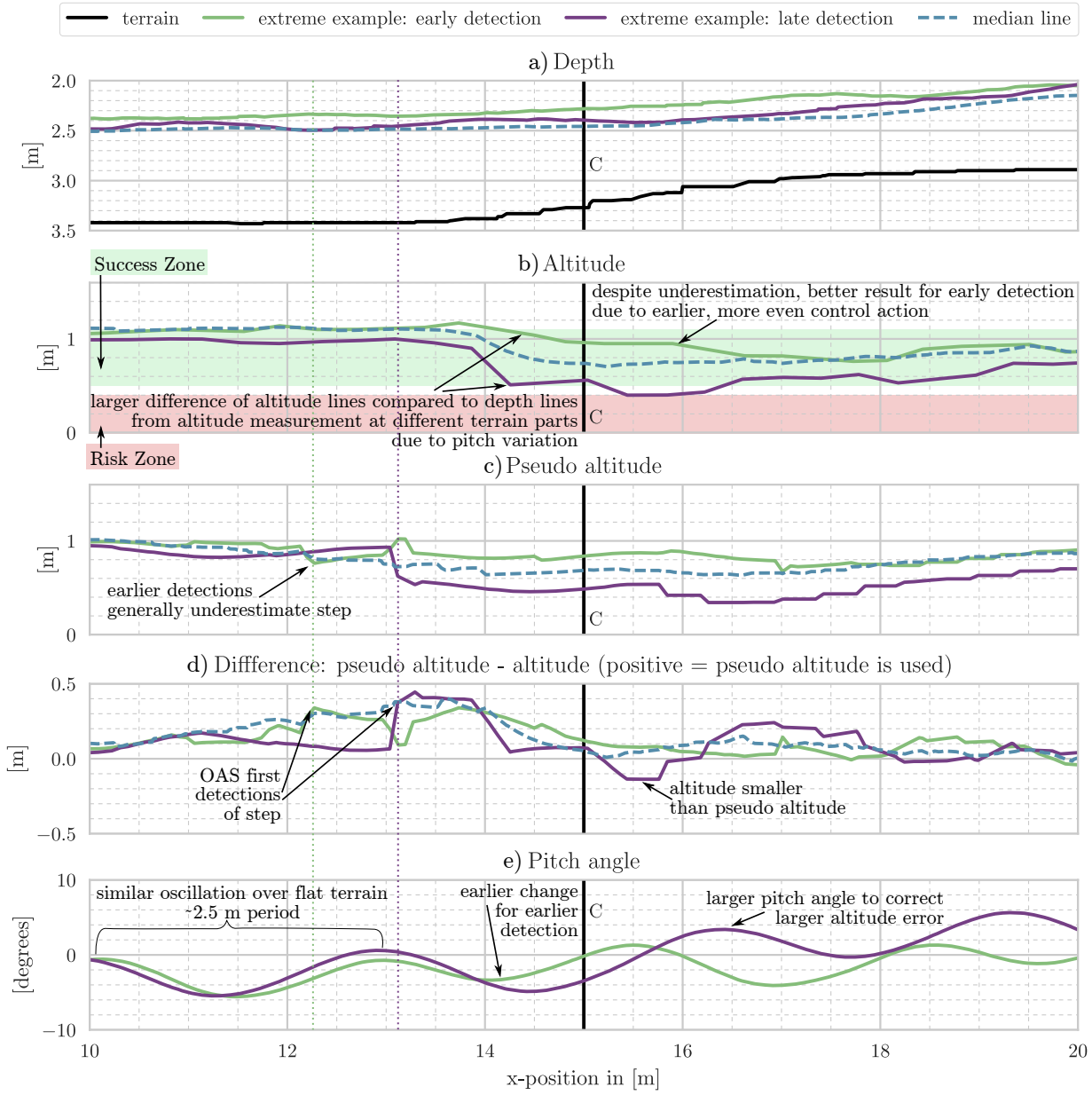

Figure 18: Extreme cases of early and late forwards detection for case 8 (1 m/s), compared to median line. The plot uses the $A \triangleright B$ direction, showing 5 m before and after the upwards step at C. Details of the impact of detection variation on altitude, pseudo altitude and pitch angle are annotated.

To estimate the overall obstacle detection success, the detection of each experiment was manually compared to the sonar scan, and categorised into three groups: no false detection, occasional false detections, and significant false detections. No false detections were found for most of the experiments with a fixed threshold S_{th} set at 95. Reducing the threshold to 85 or varying it proportionally to the distance resulted in occasional false detections for each of the experiments, and further reducing the threshold to $S_{th} = 75$ resulted in significant false detections for all experiments. Whilst it was expected that the detection would be less impacted by the surface reflections at lower altitude, due to the larger depth, the improvement was not significant.

At 1 m altitude, the detection range of the first step was on average 3 m. This distance varied by up to ± 1.4 m, as expected a 2.8 s sector scan time. The sonar settings from case 10 and 11 increased this distance to over 4 m. For a 0.6 m altitude goal, the average range is drastically reduced to between 1.5 m and 2 m. With the variation over the scan period this lead to detection ranges as low as 0.1 m. However this still presents a significant safety improvement, compensating false altimeter readings. Figure 18 compares examples of both very late and very early detection to the median line of case 8. Whilst the experiment with a late detection measures a significantly higher terrain altitude, the detection range of just above 1 m does not leave enough time for the vehicle to achieve a sufficient depth change rate, resulting in one of the highest risk results for case 8. This illustrates the importance of considering repeatability and variation in sensor performance for understanding the vehicle risk.

6.2 Actuation strategy

The impact of the transition between flight style and hover capable actuation is measurable in the distance made good until the goal altitude is reached again (without obstacle detection). It is below 3 m for 0.3 m/s hover capable control and increases to over 7 m for flight style control. Using flight style actuation only, at 1 m/s speed a significant portion of the experiments show an oscillation in the pitch angle (see Figures 16, 18) that is not observed when tracking a depth with the same controller (see (Tanakitkorn et al., 2016)). Due to the dynamics of the AUV acting as a low pass filter this oscillation is barely noticeable in the altitude and depth measurements.

Whilst the standard control for Delphin2 phases out the use of the thrusters between surge velocities of 0.8 m/s and 1.0 m/s (see Figure 14), the thruster weight was varied at maximum speed to see if the thrusters can support the flight style control for obstacle avoidance. Figure 19 compares the three 1 m/s cases with sternplane only actuation and variations of the thruster usage. The selected cases use only the altimeter for obstacle avoidance to remove timing effects from the obstacle detection. The flight style control with added thruster actuation overall maintains the goal altitude better (see Figure 20), however an impact of the thrusters on the efficiency on the pitch control can clearly be seen: Despite sternplanes set for pitching the vehicle upwards, and the expected thruster moment supporting this, the vehicle error indicates that the vehicle tends to pitch downwards more than demanded. A fast pitch change rate is still achieved at the upwards step (see altitude and pitch error plots in Figure 19), but the goal altitude is approached much slower since the vehicle soon acquires a downwards pitching error again. This contributes to a lower overshoot for the current control parameters, and reduces the time it takes to return to the goal height after a downwards step. Thus the overall results are still better for these actuation strategies, but the loss of pitch control makes them unsuitable.
The reasons behind the difficulties tracking a given pitch angle when combining the thrusters at high speed are likely a combination of the sternplanes being less efficient due to the turbulence cause by the thrusters, the thruster performance degrading with surge speed at different rates as observed in (Palmer et al., 2009). Furthermore ground effects from operating at low distances to the terrain, similar to those observed at the free surface, may play a role, though the thruster tests at up to 0.8 m/s altitude only show variations in differential pressure at larger depths (lower altitudes) for the highest thruster speeds (Steenson et al., 2011).

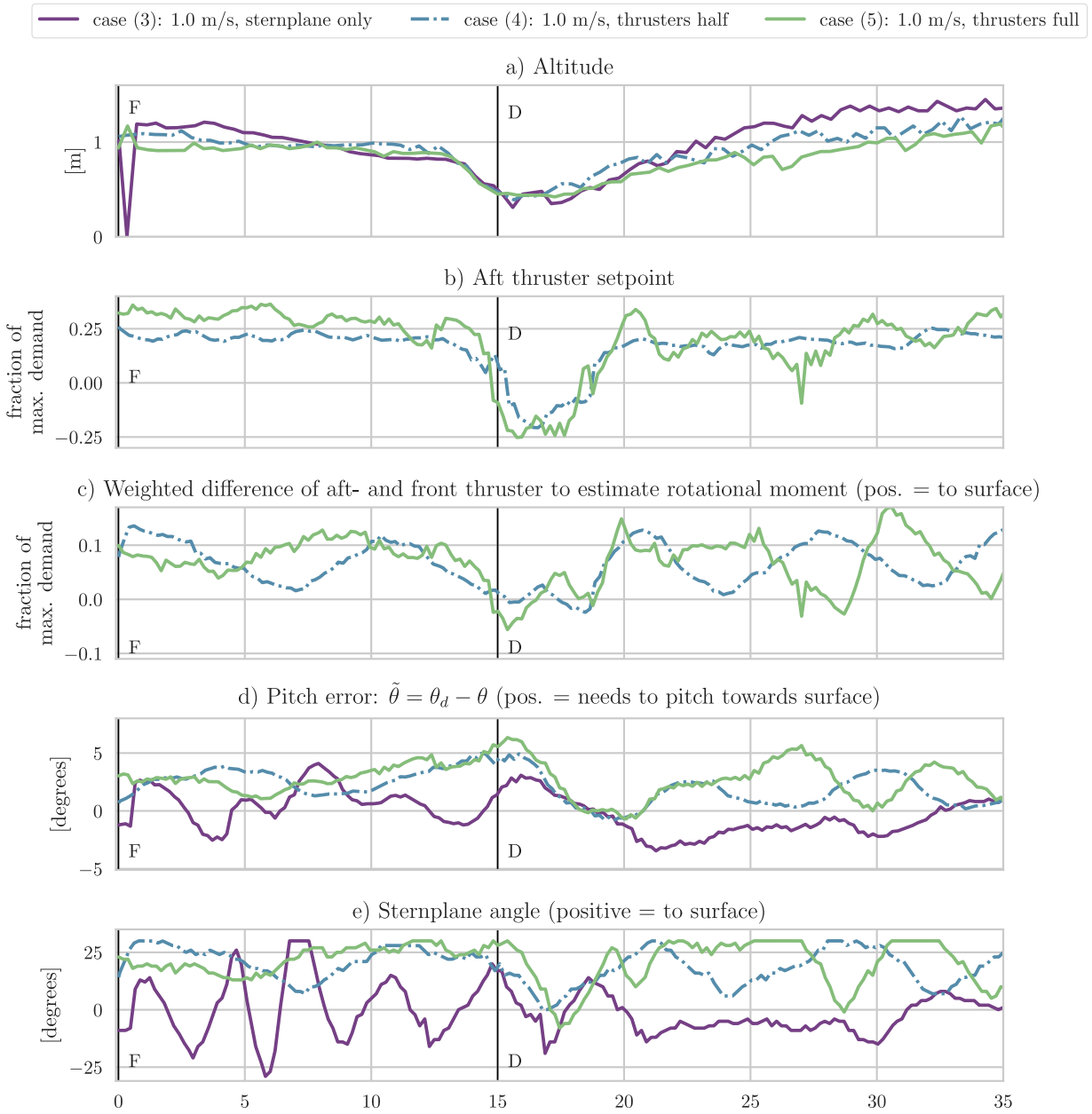

Figure 19: Using the altimeter only for tracking, and a constant surge velocity of 1 m/s, the thruster weight is varied (cases 3, 4, 5, thruster weight function variation is shown in Figure 14). The $B \triangleright A$ direction is shown, since for this direction none of the three cases had altimeter spike measurements. To estimate the pitching moment generated by the thrusters, the thruster setpoints are weighted according to their distance to the centre of rotation, and subtracted to calculate the force contributed to the pitching moment.

6.3 Altitude tracking performance

The altitude tracking performance was analysed using both the altimeter measurement directly and the altitude estimated from the depth and position over the terrain. To measure the ability of Delphin2 to keep a constant altitude over complex terrain, the mean and standard deviation of the altitude was calculated over all experiments of each case.
The two altitude estimation methods agree well overall; when the altitude estimate is used, the average altitude reduces and the vehicle risk increases in the $B \triangleright A$ direction. With this more accurate altitude estimate, several experiments in the $B \triangleright A$ direction can be identified where a collision at point D is likely due to the altitude estimate falling below 0.1 m. Once the distance of the bounding box was considered, the vehicle risk was further increased, resulting in several likely collisions for the 0.6 m altitude tracking experiments. Whilst this method of altitude estimation is unavailable for the typical terrain tracking applications, it not only illustrates the impact of the altimeter accuracy for understanding the performance, but also highlights the advantage of performing repeatable experiments over an easy to access and well mapped terrain.

Figure 20 shows that for most cases, the resulting altitude was above the goal altitude. Only the over-actuated cases 4 and 5 resulted in a mean altitude below the goal altitude. The 0.3 m/s altitude tracking without obstacle avoidance (case 1) comes closest to achieving the goal altitude. The lowest standard deviation can be found for the slower speed cases, with a standard deviation below 0.2 m. For most cases the standard deviation is smaller for the direction $A \triangleright B$. Using a fixed sonar threshold of $S_{th} = 85$ or above results in an altitude deviation below 0.5 m, whilst the remaining sonar settings (cases 10, 11, 15, and 16) clearly stand out with an altitude standard deviation above 0.5 m, and often also with the standard deviation larger for the $A \triangleright B$ direction, indicating a failure to detect the terrain ahead.

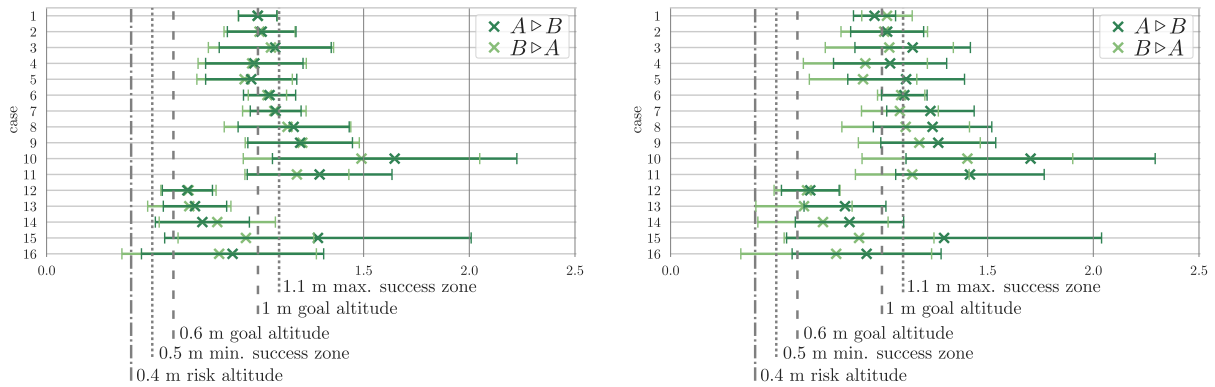

Figure 20: Mean altitude and standard deviation of that altitude for all configurations.

Figures 21 and 22 show the success and risk results for the individual experiments, since for most cases the number of repeats is not sufficient to make statistical assessments. Considering only the risk and photo success numbers, the best performance is found for cases 1, 2, and 4, with a mission risk of less than 5% and a success rate above 60%. All cases use thruster actuation, but the success of case 4 has been shown to be due to control problems rather than effective altitude tracking. The tendency to stay above the goal altitude when using flight style actuation is clearly indicated in the mission success as well. All attempts at tracking the 1 m goal altitude with flight style actuation and forwards looking capabilities result in a mission success below 50% (Cases 8, 9, 10, 11) , conforming with their mean altitude above the mission success zone. Whilst using the direct altitude measurement, comes as a surprise that the added forwards looking capability increases the vehicle risk for the 0.3 m/s at 1 m altitude experiments (cases 1 and 6), however with a reduced risk for the bounding box analysis this is likely due to sensor errors. The majority of the forwards scanning experiments at 1 m/s have a very low mission risk. In the reverse direction, the reference case 8 still

shows several experiments with a similar risk factor to that of the 1 m/s altitude tracking without forwards looking obstacle avoidance. Based on the obstacle detection analysis, these are cases where the timing of the scanning sonar lead to a late detection of the step. Considering the total number of experiments of the reference case, the risk is still significantly reduced by using forwards looking obstacle avoidance, whilst accepting a reduction in mission success.

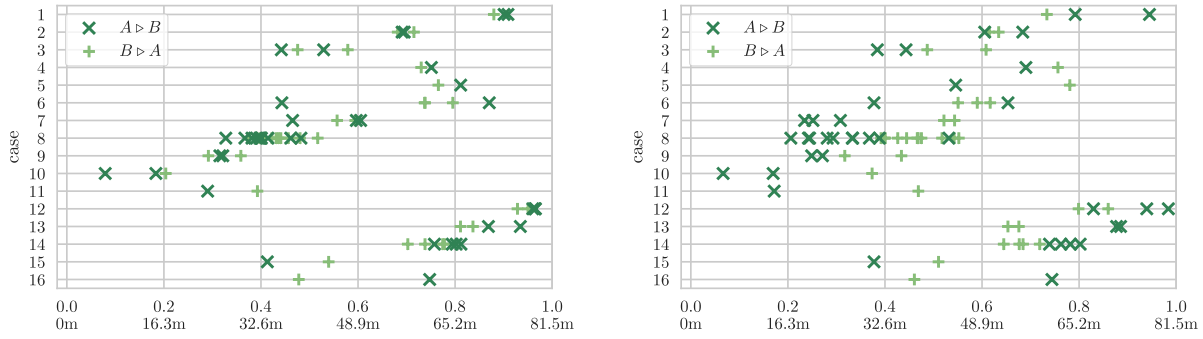

(a) (b)

Figure 21: Comparison of the mission success results for all experiment cases. Mission success is given as a proportion of the distance spent in the success zone relative to the full mission path length, and as the length of the distance spent in the success zone in metres.

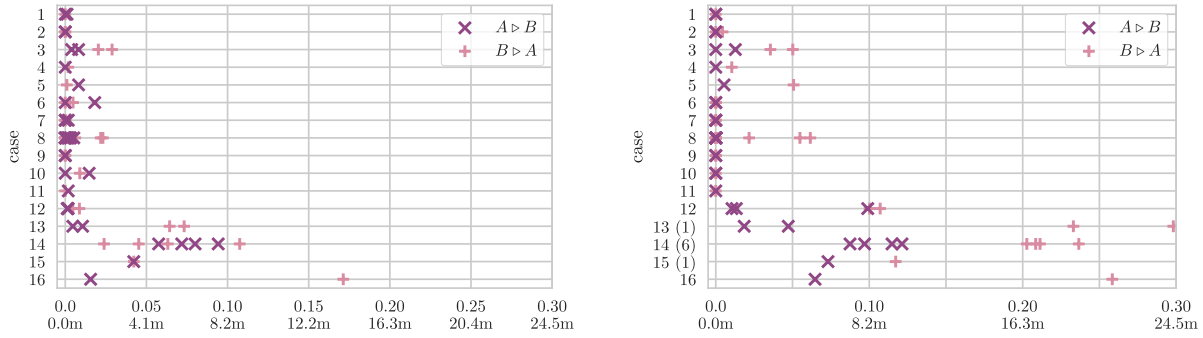

(a) (b)

Figure 22: Comparison of the vehicle risk and the impact of the altimeter limits. Mission risk is given as a proportion of the distance spent below 0.4 m altitude relative to the full mission path length, and as the length of the distance spent in the success zone in metres.

6.4 Cost of transport

For any mission plan, the power consumption is a major factor that needs consideration. This section compares the average power use of the different terrain tracking cases, the resulting successfully covered study area and the impact of the terrain complexity on the energy consumption by the actuators.

The total energy used during one experiment is calculated by integrating the product of the supply voltage and the current drawn over each time step. The average power consumption is the total energy used divided by the total time. The battery voltage as well as the current drawn by the individual thrusters, the control surfaces, and the propeller are logged at rate of 0.5 Hz. The hotel load is estimated at 30 W (Tanakitkorn et al., 2016), based on the current drawn when running Delphin2 directly from a power supply. Based on

the style of propulsion a variation in power usage can be observed but it is less than expected since the power use mostly shifts between the propeller and the thrusters (see Figure 24), with a variation of less that 15% around the average value of 71.7 W. The minimal average power is consumed during 1 m/s flight style propulsion, the maximum average power during thruster enhanced flight style control and during 0.6 m/s hover capable control. Figure 24(a) shows the average power usage of one experiment, the 81.5 m distance between E and F, for examples of cases with low (8), medium (6) and high (3, 7) average power consumption.

The average power consumption misses one key information for understanding mission performance: It does not take the distance covered into consideration. A normalised measure that considers the energy required to move a vehicle by a unit distance is the cost of transport (COT) (Phillips et al., 2017).

$$COT\left[\frac{J}{m \cdot kg}\right] = \frac{\text{Energy}[J]}{\text{Distance}[m] \cdot \text{Mass}[kg]} \tag{3}$$

Delphin2 has a mass of 79.40 kg, the energy available is estimated as:

$$\begin{aligned} E_{battery} &= \text{Number of cells} \cdot \text{Nominal Voltage} \cdot \text{Battery capacity} \\ &= 3 \cdot 21.6V \cdot 10Ah \\ &= 2333kJ \end{aligned} \tag{4}$$

Compared to cost of transport of depth tracking at different speeds in (Tanakitkorn et al., 2016), the cost of transport for altitude tracking increases around 10% for flight style actuation, 20% for hover capable actuation, and 20% for flight style actuation with thruster use.
For hover capable control, the thrusters are both used for generating a pitching moment and vertical translation. The variation due to generating a pitching moment is differential between the two thrusters, whilst that for vertical translation is additive. Depending on which of the two is dominant, either the change rate of the slope (= correction of pitch angle), or the slope (= altitude correction) will have a larger impact on the variation power consumption. In terms of power, an altitude correction will always lead to an according change in power consumption; a pitch angle correction may be a zero change by varying the thrusters differentially, but an upper limit can be estimated by taking the difference between the thruster demands and assuming that only one of the thrusters changes its setting. To analyse which of the two is dominant in the current control scheme for Delphin2, the standard deviation of the sum and difference of the actuator power consumption was analysed. Overall, the translation was always found dominant, with varying extent between the cases. Figure 23 demonstrates that the variation in the sum of both thrusters is indeed well aligned with the altitude error. For a positively buoyant vehicle like Delphin2 this means a reduced power demand for a negative altitude error and vice versa. As a result the average power demand increases for a downwards sloping terrain and reduces on an upwards slope. A difference in power consumption between the different altitude tracking methods or the two directions could not be distinguished.
Since the sternplane actuation on Delphin2 is not proportional to the required force, the direction of the slope has no influence and the 10% increase is only due to the increased length of the vehicle path relative to the progress made in x-direction.

For comparison to other vehicles, the energy consumption is combined with the mission risk and success measures, to estimate how much distance can be successfully surveyed during one mission. Such an overview is given in Table 3. However, these numbers are terrain specific, due to the lack of a suitable measure for comparing terrain complexity, in particular when considering the difference in diving and surfacing performance of positively buoyant vehicles regarding both slope and step height.

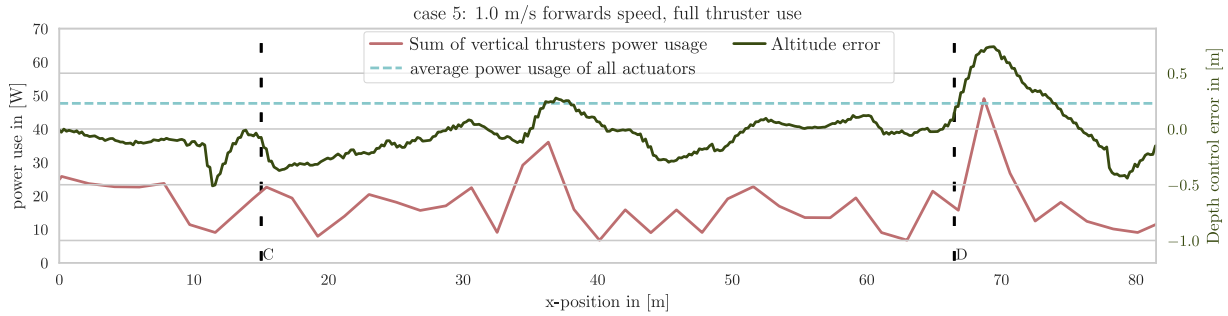

Figure 23: Correspondance between altitude error and thruster power consumption.

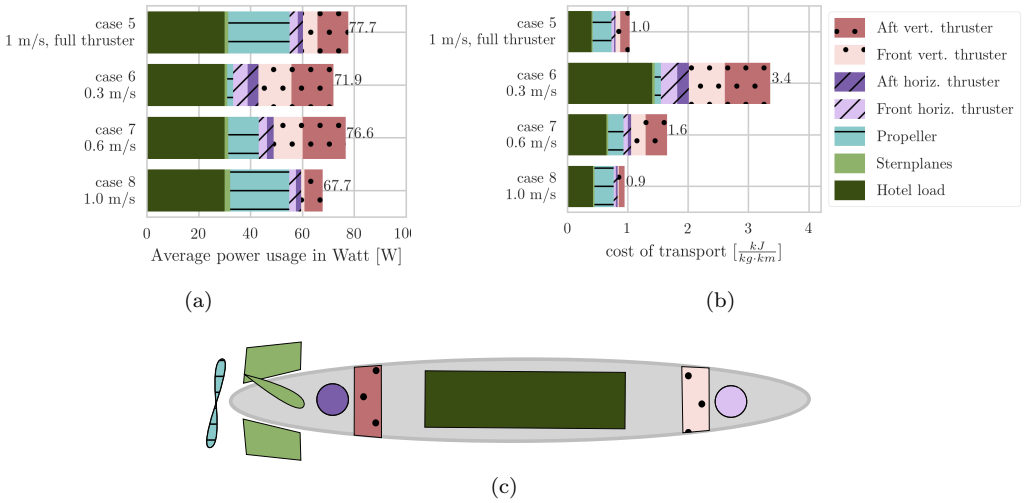

Figure 24: Comparison of the average power consumption and cost of transport for 0.3 m/s, 0.6 m/s, and 1 m/s with default configuration and 'full thruster' configuration, using experiment cases 5, 6, 7, and 8.

7 Conclusion

This paper has undertaken a detailed analysis of AUV terrain following, using data from repeated experiments over the same terrain to compare altitude tracking success and repeatability for different configurations. For reliable terrain detection, the altitude tracking was shown to be repeatable, with a distinction in the results for different actuation and control methods. Whilst some changes had to be made for the obstacle detection, the repeatable and cost efficient experiment set-up on Delphin2 was demonstrated as a valuable tool, directing the focus of the analysis of Autosub6000 data towards the forwards looking detection and the stability of the altitude control. The results are presented with sufficient information to be transferable to other hover capable or flight style AUVs.

As expected, the best altitude tracking performance with minimum variation in pitch angle was observed for hover capable actuation at slow speed. With the transition to more energy efficient flight style actuation, the slower reactions of the vehicle reduces the altitude tracking capability. At this point the forwards looking obstacle avoidance system becomes crucial for minimising collision risk. It was shown how the impact of the forwards detection on vehicle safety is constrained by the detection rate and range of the mechanical scanning sonar.

Increasing the forwards speed of the vehicle increases the area that can be surveyed. The mission success rates show that this effect deprecates with increased terrain complexity and unreliable terrain detection. The error in altitude increases especially on a downwards slope or step. Further increasing risk and reducing the photo

quality, no steady state pitch angle was reached with the current controller. It was found that the addition of thrusters at full speed does not improve the altitude tracking capabilities, but reduces controllability of the AUV.
The analysis of the experiment results demonstrates how the introduction of a risk zone in the altitude tracking analysis can show vehicle risks that may not be visible from altitude plots and statistical analysis directly, and that the mission success zone can help translate the results into more meaningful information for mission planners. Rather than choosing a flight style or hover capable vehicle, a choice is made between increased or minimal vehicle risk, larger or smaller area covered, lowered photo density or almost complete area coverage, and lower versus higher operational cost.

Future work on combining hover and flight style actuation for altitude tracking may focus on optimising energy consumption by varying the surge velocity based on the altitude error. The most significant improvements of survey results are expected from improving the terrain detection, and improving the altitude control for the downwards slope. Limited by software protocol and mechanical factors rather than the speed of sound in water, significant speed improvements may be possible by choosing a multibeam sonar over the mechanical scanning device. This will also increase the repeatability of experiments, since it removes the impact of the relative timing of the scan angle.
Improving the ability to better compare the altitude tracking performance over complex terrain not only directly impacts the choices of vehicle operators, but will also support a complete automation of the process for adaptive missions planning.

8 Acknowledgements

This work is funded by the National Oceanography Centre and the University of Southampton. Gratitude is also extended to S. Lemaire, A. R. P. Lynn and T. Schneider for their assistance at the lakeside.

References

Akkaynak, D., Treibitz, T., Shlesinger, T., Loya, Y., Tamir, R., and Iluz, D. (2017). What is the Space of Attenuation Coefficients in Underwater Computer Vision? In *2017 IEEE Conference on Computer Vision and Pattern Recognition (CVPR)*, pages 568–577. IEEE.

Becker, J. J., Sandwell, D. T., Smith, W. H. F., Braud, J., Binder, B., Depner, J., Fabre, D., Factor, J., Ingalls, S., Kim, S.-h., Ladner, R., Marks, K., Nelson, S., Trimmer, R., Rosenberg, J. V., Wallace, G., Weatherall, P., Trimmer, R., Rosenberg, J. V., Wallace, G., and Bathymetry, P. W. G. (2009). Global Bathymetry and Elevation Data at 30 Arc Seconds Resolution : SRTM30 _ PLUS Global Bathymetry and Elevation Data at 30 Arc Seconds Resolution : SRTM30 PLUS. 0419.

Bingham, B., Foley, B., Singh, H., Camilli, R., Delaporta, K., Eustice, R., Mallios, A., Mindell, D., Roman, C., and Sakellariou, D. (2010). Robotic Tools for Deep Water Archeology: Surveying an Ancient Shipwreck with an Autonomous Underwater Vehicle. *Journal of Field Robotics*, 27(6):702–717.

Bodenmann, A., Thornton, B., Nakajima, R., Yamamoto, H., and Ura, T. (2013). Wide Area 3D Seafloor Reconstruction and its Application to Sea Fauna Density Mapping. In *Proceedings of MTS/IEEE Oceans*, volume 13, pages 130006–130504.

Chew, J. L. and Chitre, M. (2013). Object Detection with Sector Scanning Sonar. In *Oceans-San Diego*, pages 1–8, San Diego. IEEE.

Dunbabin, M., Roberts, J., Usher, K., Winstanley, G., and Corke, P. (2005). A hybrid AUV design for shallow water reef navigation. In *Proceedings - IEEE International Conference on Robotics and Automation*, volume 2005, pages 2105–2110.

Eng, T. H. and Chitre, M. (2015). Minimum Speed Seeking Control for Nonhovering Autonomous Underwater Vehicles. *J. Field Robotics*, 33(5):706–733.

Furlong, M. E., McPhail, S. D., and Pebody, M. (2009). A New Collision Avoidance System for the Autosub6000 Autonomous Underwater Vehicle.

Gracias, N., Ridao, P., Garcia, R., Escartin, J., L'Hour, M., Cibecchini, F., Campos, R., Carreras, M., Ribas, D., Palomeras, N., Magi, L., Palomer, A., Nicosevici, T., Prados, R., Hegedus, R., Neumann, L., De Filippo, F., and Mallios, A. (2013). Mapping the Moon: Using a lightweight AUV to survey the site of the 17th century ship 'La Lune'. *OCEANS 2013 MTS/IEEE Bergen: The Challenges of the Northern Dimension*.

Harris, P. T., Macmillan-Lawler, M., Rupp, J., and Baker, E. K. (2014). Geomorphology of the oceans. *Marine Geology*, 352:4–24.

Haywood, R. M. (1986). Acquisition of a micro scale photographic survey using an autonomous submersible. *Oceans'86*, pages 1423–1426.

Houts, S. E. and Rock, S. M. (2015). Trajectory planning for motion-constrained AUVs in uncertain environments. *2014 Oceans - St. John's, OCEANS 2014*.

Houts, S. E., Rock, S. M., and McEwen, R. (2012). Aggressive terrain following for motion-constrained auvs. In *Autonomous Underwater Vehicles (AUV), 2012 IEEE/OES*, pages 1–7. IEEE.

Jaffe, J. S. (1990). Computer modeling and the design of optimal underwater imaging systems. *Oceanic Engineering, IEEE Journal of*, 15(2):101–111.

Kimber, N. I. and Marshfield, W. B. (1993). Design and Testing of Control Surfaces for the Autosub Demonstrator Test Vehicle.

Ling, S. D., Mahon, I., Marzloff, M. P., Pizarro, O., Johnson, C. R., and Williams, S. B. (2016). Stereo-imaging AUV detects trends in sea urchin abundance on deep overgrazed reefs. *Limnology and Oceanography: Methods*, 14(5):293–304.

Marouchos, A., Muir, B., Babcock, R., and Dunbabin, M. (2015). A shallow water AUV for benthic and water column observations. In *MTS/IEEE OCEANS 2015 - Genova: Discovering Sustainable Ocean Energy for a New World*.

McKinney, W. (2010). Data Structures for Statistical Computing in Python. *Proceedings of the 9th Python in Science Conference*, 1697900(Scipy):51–56.

McPhail, S. D. (2010). RSS Discovery Cruise 343: Deepwater trials of the Autosub6000 AUV, HyBIS, and telemetry systems.

McPhail, S. D., Furlong, M., and Pebody, M. (2010). Low-altitude terrain following and collision avoidance in a flight-class autonomous underwater vehicle. *Proceedings of the Institution of Mechanical Engineers, Part M: Journal of Engineering for the Maritime Environment*, 224(4):279–292.

McPhail, S. D. and Pebody, M. (1998). Navigation and control of an autonomous underwater vehicle using a distributed, networked, control architecture. *Underwater Technology*, 23(1):19–30.

Morris, K. J., Bett, B. J., Durden, J. M., Huvenne, V. A. I., Milligan, R., Jones, D. O. B., McPhail, S., Robert, K., Bailey, D. M., and Ruhl, H. A. (2014). A new method for ecological surveying of the abyss using autonomous underwater vehicle photography. *Limnology and Oceanography: Methods*, 12:795–809.

Nakajima, R., Yamamoto, H., Kawagucci, S., Takaya, Y., Nozaki, T., Chen, C., Fujikura, K., Miwa, T., and Takai, K. (2015). Post-Drilling Changes in Seabed Landscape and Megabenthos in a Deep-Sea Hydrothermal System, the Iheya North Field, Okinawa Trough. *PLoS ONE*, 10(4).

Nishida, Y., Nagahashi, K., Sato, T., Bodenmann, A., Thornton, B., Asada, A., and Ura, T. (2015). Development of an autonomous underwater vehicle for survey of cobalt-rich manganese crust. *OCEANS 2015 - MTS/IEEE Washington*, pages 0–4.

Nishida, Y., Tamaki, U., Hamatsu, T., Nagahashi, K., Inaba, S., and Nakatani, T. (2014a). Investigation method for the biomass of kichiji rockfish by hovering type AUV. In *OCEANS 2014 - TAIPEI*, pages 1–4.

Nishida, Y., Ura, T., Hamatsu, T., Nagahashi, K., Inaba, S., and Nakatani, T. (2014b). Resource investigation for Kichiji rockfish by autonomous underwater vehicle in Kitami-Yamato bank off Northern Japan. *ROBOMECH Journal*, 1(1):1–6.

Otsuki, Y., Thornton, B., Maki, T., Nishida, Y., Bodenmann, A., and Nagano, K. (2016). Real-time Autonomous Multi Resolution Visual Surveys Based on Seafloor Scene Complexity. pages 330–335.

Packard, G. E., Stokey, R., Christenson, R., Jaffre, F., Purcell, M., and Littlefield, R. (2010). Hull inspection and confined area search capabilities of REMUS autonomous underwater vehicle. *MTS/IEEE Seattle, OCEANS 2010*, (October).

Palmer, A., Hearn, G. E., and Stevenson, P. (2009). Experimental Testing of an Autonomous Underwater Vehicle with Tunnel Thrusters. In *First International Symposium on Marine Propulsion*, number June, pages 1–6.

Pebody, M. (2008). Autonomous underwater vehicle collision avoidance for under-ice exploration. *Proceedings of the Institution of Mechanical Engineers, Part M: Journal of Engineering for the Maritime Environment*, 222(2):53–66.

Phillips, A. B., Haroutunian, M., Murphy, A. J., Boyd, S. W., Blake, J. I., and Griffiths, G. (2017). Understanding the power requirements of autonomous underwater systems, Part I: An analytical model for optimum swimming speeds and cost of transport. *Ocean Engineering*, 133:271–279.

Phillips, A. B., Steenson, L. V., Rogers, E., Turnock, S. R., Harris, C., and Furlong, M. (2013). Delphin2: An over actuated autonomous underwater vehicle for manoeuvring research. *Transactions of the Royal Institution of Naval Architects Part A: International Journal of Maritime Engineering*, 155(PART A4).

Phillips, A. B., Turnock, S. R., and Furlong, M. (2010). The use of computational fluid dynamics to aid cost-effective hydrodynamic design of autonomous underwater vehicles. *Proceedings of the Institution of Mechanical Engineers Part M: Journal of Engineering for the Maritime Environment*, 224(4):239–254.

Roman, C. and Mather, R. (2010). Autonomous underwater vehicles as tools for deep-submergence archaeology. *Proceedings of the Institution of Mechanical Engineers Part M: Journal of Engineering for the Maritime Environment*, 224(4):327–340.

Ruhl, H. A. (2013). RRS Discovery Cruise 377 & 378: Autonomous ecological surveying of the abyss: understanding mesoscale spatial heterogenety at the Porcupine Abyssal Plain.

Schillai, S. M., Turnock, S. R., Rogers, E., Phillips, A. B., and Harris, C. A. (2016). Evaluation of Terrain Collision Risks for Flight Style Autonomous Underwater Vehicles. In *IEEE/OES Autonomous Underwater Vehicles (AUV)*, pages 311–318, Tokyo.

Singh, H., Armstrong, R., Gilbes, F., Eustice, R., Roman, C., Pizarro, O., and Torres, J. (2004a). Imaging Coral I: Imaging Coral Habitats with the SeaBED AUV. *Subsurface Sensing Technologies and Applications*, 5(1):25–42.

Singh, H., Can, A., Eustice, R., Lerner, S., McPhee, N., Pizarro, O., and Roman, C. (2004b). Seabed AUV Offers New Platform for High-Resolution Imaging. *Eos, Transactions American Geophysical Union*, 85(31):160.

Smale, D. A., Kendrick, G. A., Harvey, E. S., Langlois, T. J., Hovey, R. K., Niel, K. P. V., Waddington, K. I., Bellchambers, L. M., Pember, M. B., Babcock, R. C., Vanderklift, M. A., Thomson, D. P., Jakuba, M. V., Pizarro, O., and Williams, S. B. (2012). Regional-scale benthic monitoring for ecosystem-based fisheries management (EBFM) using an autonomous underwater vehicle (AUV). *ICES Journal of Marine Science*, 69:1108–1118.

Steenson, L. V., Phillips, A. B., Furlong, M. E., Rogers, E., and Turnock, S. R. (2011). The performance of vertical tunnel thrusters on an autonomous underwater vehicle operating near the free surface in waves. *Second International Symposium on Marine Propulsors*, (June):1–8.

Steenson, L. V., Turnock, S. R., Phillips, A. B., Harris, C., Furlong, M. E., Rogers, E., Wang, L., Bodles, K., and Evans, D. (2014). Model predictive control of a hybrid autonomous underwater vehicle with experimental verification. *Proceedings of the Institution of Mechanical Engineers, Part M: Journal of Engineering for the Maritime Environment*, 228(2):166–179.

Tanakitkorn, K., Wilson, P. A., Turnock, S. R., and Phillips, A. B. (2016). Depth Control for an Over-Actuated , Hover-Capable Autonomous Underwater Vehicle with Experimental Verification. *Mechatronics*, 41:67–81.

Tanakitkorn, K., Wilson, P. A., Turnock, S. R., and Phillips, A. B. (2017). Sliding Mode Heading Control of an Over-Actuated , Hover-Capable Autonomous Underwater Vehicle with Experimental Verification. *Journal of Field Robotics*, 35(3):396–415.

Tolimieri, N., Clarke, M., Singh, H., and Goldfinger, C. (2008). Evaluating the SeaBED AUV for Monitoring Groundfish in Untrawlable Habitat. *Marine Habitat Mapping Technology for Alaska*, pages 129–142.

Tritech International Ltd. Micron Echosounder Ultra Compact Underwater Altimeter.

Williams, S., Pizarro, O., Jakuba, M., and Barrett, N. (2010a). AUV benthic habitat mapping in south eastern Tasmania. *Field and Service Robotics*, 62:275–284.

Williams, S. B., Pizarro, O., Howy, M., Mercer, D., Powell, G., Marshally, J., and Hanlon, R. (2009a). Surveying noctural cuttlefish camouflage behaviour using an AUV. *Proceedings - IEEE International Conference on Robotics and Automation*, pages 214–219.

Williams, S. B., Pizarro, O., Jakuba, M. V., Mahon, I., Ling, S. D., and Johnson, C. R. (2010b). Repeated AUV surveying of urchin barrens in north eastern Tasmania. *Proceedings - IEEE International Conference on Robotics and Automation*, pages 293–299.

Williams, S. B., Pizarro, O. R., Mahon, I., and Johnson-Roberson, M. (2009b). Simultaneous localisation and mapping and dense stereoscopic seafloor reconstruction using an AUV. *Experimental robotics*, pages 407–416.

Woolsey, M., Asper, V. L., and Mcletchie, K. (2009). Enhancing NIUST ' s SeaBED Class AUV , Mola Mola. *Autonomous Underwater Vehicles (AUV), 2010 IEEE/OES*, pages 1–5.

Wynn, R. B., Huvenne, V. A. I., Le Bas, T. P., Murton, B. J., Connelly, D. P., Bett, B. J., Ruhl, H. A., Morris, K. J., Peakall, J., Parsons, D. R., Sumner, E. J., Darby, S. E., Dorrell, R. M., and Hunt, J. E. (2014). Autonomous Underwater Vehicles (AUVs): their past, present and future contributions to the advancement of marine geoscience. *Marine Geology*, 352:451–468.

Yoerger, D. R., Bradley, A. M., and Walden, B. B. (1991). The autonomous benthic explorer (ABE): An AUV optimized for deep seafloor studies. *Proceedings of the 7th International Symposium on Unmanned Untethered Submersible Technology*, pages 75–85.

Yoerger, D. R., Jakuba, M., Bradley, A. M., and Bingham, B. (2007). Techniques for deep sea near bottom survey using an autonomous underwater vehicle. *International Journal of Robotics Research*, 26(1):41–54.

Zhou, M., Bachmayer, R., and Deyoung, B. (2016). Mapping for control in an underwater environment using a dynamic inverse-sonar model. In *OCEANS 2016 MTS/IEEE Monterey, OCE 2016*.

Tables

	Autosub 6000	Delphin2
Vehicle length L	5.5 m	1.96 m
Mission parameters		
Min. goal altitude	3 m	0.6 m
Max. goal altitude	10 m	1.0 m
Surge velocity	1.5 m/s	1.0 m/s
Sonar		
Horizon tracking update time t	1.3 s	0.8 s
Time between continuous scan measurements	-	0.02 s
Lower sector scan time	16 s	2.8 s
Step size	3^o	3.6^o
Vertical beam opening angle	3^o	3^o
Horizontal beam opening angle	20^o	35^o
Low Altitude Detection Range	150 m	4 m
Blanking distance	5 m	0.6 m

Table 1: Dimensional and non-dimensional key scales of the experiments with Autosub6000 and Delphin2

Case No.	Altitude		Speed			Thrusters		Detection		Repeats	
	$0.6m$	$1.0m$	$0.3\frac{m}{s}$	$0.6\frac{m}{s}$	$1.0\frac{m}{s}$	original	varied	S_{th}	S_r	$A \triangleright B$	$B \triangleright A$
1)		■	■			■				2	1
2)		■		■		■				2	2
3)		■			■	■				2	2
4)		■			■		half			1	1
5)		■			■		full			1	1
6)		■	■			■		95		2	3
7)		■		■		■		95		3	2
8)		■			■	■		95		10	11
9)		■			■	■		85		2	2
10)		■			■	■		75		2	1
11)		■			■	■		95	1	1	1
12)	■		■			■		95		3	2
13)	■			■		■		95		2	2
14)	■				■	■		95		4	4
15)	■				■	■		75		1	1
16)	■				■	■		95	1	1	1

Table 2: Experiment Matrix for Testwood Lake experiments. An empty detection threshold S_{th} in the obstacle detection indicates that only the altimeter was used for obstacle avoidance. Repeats vary due to time limitations at the lake not allowing for all missions with a mission abort to be re-run.

Case No.	Altitude [m]	Speed $\frac{m}{s}$	Thruster weight	Detection s_{th}	s_r	[km] per hour Distance	Success	Risk	[km] per Battery charge Distance	Success	Risk
1)	1.0	0.3	original			1.1	1.0	0.0	7.9	7.0	0.0
2)	1.0	0.6	original			2.2	1.6	0.0	14.6	10.3	0.0
3)	1.0	1.0	original			3.6	1.7	0.2	27.3	12.9	1.2
4)	1.0	1.0	half			3.6	2.7	0.0	25.1	19.0	0.3
5)	1.0	1.0	full			3.6	2.2	0.2	25.3	15.7	1.3
6)	1.0	0.3	original	95		1.1	0.7	0.0	7.7	4.6	0.0
7)	1.0	0.6	original	95		2.2	0.7	0.0	15.8	5.1	0.0
8)	1.0	1.0	original	95		3.6	1.3	0.0	27.1	10.1	0.4
9)	1.0	1.0	original	85		3.6	1.1	0.0	29.5	9.3	0.0
10)	1.0	1.0	original	75		3.6	0.4	0.0	29.0	3.4	0.0
11)	1.0	1.0	original	95	1	3.6	0.7	0.0	28.4	5.7	0.0
12)	0.6	0.3	original	95		1.1	1.0	0.1	7.4	6.7	0.8
13)	0.6	0.6	original	95		2.2	2.0	0.6	15.8	14.3	4.2
14)	0.6	1.0	original	95		3.6	2.9	0.8	28.6	23.4	6.1
15)	0.6	1.0	original	75		3.6	1.3	0.4	26.0	9.2	3.0
16)	0.6	1.0	original	95	1	3.6	2.8	0.9	27.5	21.1	7.1

Table 3: Estimated performance for a day long mission and for one battery charge.